Computational Study of Environmental Effects in the Adsorption of DMMP, Sarin, and VX on γ-Al_2O_3: Photolysis and Surface Hydroxylation

V. M. Bermudez*

Electronics Science and Technology Division, Naval Research Laboratory, Washington, D.C. 20375-5347

Received: October 13, 2008; Revised Manuscript Received: November 28, 2008

The adsorption of the chemical warfare agent simulant dimethyl methylphosphonate (DMMP) and the real agents Sarin and VX on the γ-Al_2O_3 surface has been studied using density functional theory. The focus is primarily on two different environmental effects, namely, surface hydroxylation and photoexcitation due to terrestrial solar radiation. Cluster models for the hydroxylated surface have been examined in detail, focusing on the chemical and electronic structure. The energy for formation via dissociative adsorption of H_2O, the density of states of the occupied cluster orbitals and the OH deprotonation energies have been compared with results from two-dimensionally periodic slab calculations and, where available, with experimental data. For all three species, adsorption on an OH-free surface occurs via an Al(T_d)—O═P dative bond to an unsaturated tetrahedral Al(T_d) site. For the hydroxylated surface, OH sites which are 3-fold coordinated to Al are more reactive than one-fold coordinated sites, in agreement with experiment. In hydrogen-bond formation, the phosphonyl O atom is favored over other active centers (e.g., an alkoxy O atom); however, dative bonding remains the most stable mode of adsorption when OH-free Al(T_d) sites are available. The tertiary amine group in VX is found to be sufficiently basic to extract an H^+ from an acidic OH site. Even on a fully-OH-covered surface, only a single OH—O═P bond is formed, together with weaker CH—O bonds involving alkyl groups. These have been analyzed using the Atoms in Molecules theory. The threshold for electronic excitation of DMMP or Sarin, either in the gas phase or adsorbed on γ-Al_2O_3, is found to occur in the vacuum-ultraviolet, well beyond the upper limit of the terrestrial solar spectrum ($\sim$4.5 eV). For VX, on the other hand, the threshold is at $\sim$4.2 eV in the gas phase and shifts slightly to the red when adsorbed. Adsorption-induced shifts in the threshold transition energies have been analyzed in terms of those in the initial and final states.

1. Introduction

The application of quantum-chemical methods to the study of the phosphonyl-based chemical warfare agents (CWAs) has attracted a significant amount of attention.[1−25] This has been driven by practical considerations and by the severe difficulties inherent in experiments with real CWAs. The species thus studied include Tabun[8,22] (GA), Sarin[4−6,10−12,15,17−21,23−25] (GB), Soman[2,4,10,11,17,19,21] (GD), VX[1,3,7,9,13,14,16] and their analogs. The simulant dimethyl methylphosphonate (DMMP) has also been studied computationally.[23−31] Of particular interest are the interactions of CWAs with the surfaces of materials. This is an important issue in CWA detection, protection and remediation and in understanding agent fate, i.e., the behavior of adsorbed CWAs during exposure to the environment.[32]

To date, quantum-chemical work on the interaction of CWAs with materials has focused mainly on the adsorption of Sarin on clays, minerals, and oxides.[19−25] The interest here has been in determining the structure and energetics of the adsorbate and in comparing observed and calculated infrared (IR) vibrational spectra. Much of this work has involved ideal surfaces which are free of foreign species. However real oxide surfaces exposed to the environment are usually covered with chemisorbed H_2O (i.e., OH groups) and physisorbed molecular H_2O. This aspect has received less attention. To our knowledge the only ab initio investigations for hydroxylated ionic metal oxides have been those of Michalkova et al.[20,22,26] which addressed the adsorption of Tabun, Sarin, and DMMP on MgO and CaO both with and without coadsorbed OH. It was found that OH can promote the partial dissociation of Sarin adsorbed on MgO through the elimination of an HF molecule; whereas, the interaction of Tabun with hydroxylated CaO is weak.

The present work examines the behavior, on the hydroxylated γ-Al_2O_3 surface, of DMMP, Sarin, and VX (Figure 1). There are two main objectives. First we wish to determine the extent to which hydroxylation of the γ-Al_2O_3 surface affects adsorption, in comparison to the behavior of the OH-free surface. Sufficient data are available (see below) for adsorption of these reagents on γ-Al_2O_3 to permit some degree of comparison between observed and calculated results. This effort will require careful attention to the details underlying the construction of a suitable model for the hydroxylated γ-Al_2O_3 surface. Included in this is a comparison with results[24] for adsorption on hydroxylated amorphous silica (a-SiO_2). Second, as a step toward the systematic understanding of issues relating to agent fate, we are interested in comparing the electronic excitation of each species in the free and adsorbed states. This is relevant to possible photochemical effects when CWAs are exposed to sunlight. The absorption spectra of CWAs and simulants in the near-ultraviolet (UV) have not been widely studied. Hence, an ability to predict this property, and the effect of adsorption, would be a valuable asset in understanding agent fate. This work is also, to our knowledge, the first computational study of the adsorption of VX on any material.

* To whom correspondence should be addressed. E-mail: victor.bermudez@nrl.navy.mil. Phone: +1-202-767-6728. Fax: +1-202-767-1165.

10.1021/jp809053u This article not subject to U.S. Copyright. Published 2009 by the American Chemical Society
Published on Web 01/08/2009

Report Documentation Page

Form Approved
OMB No. 0704-0188

Public reporting burden for the collection of information is estimated to average 1 hour per response, including the time for reviewing instructions, searching existing data sources, gathering and maintaining the data needed, and completing and reviewing the collection of information. Send comments regarding this burden estimate or any other aspect of this collection of information, including suggestions for reducing this burden, to Washington Headquarters Services, Directorate for Information Operations and Reports, 1215 Jefferson Davis Highway, Suite 1204, Arlington VA 22202-4302. Respondents should be aware that notwithstanding any other provision of law, no person shall be subject to a penalty for failing to comply with a collection of information if it does not display a currently valid OMB control number.

1. REPORT DATE	2. REPORT TYPE	3. DATES COVERED
NOV 2008		**00-00-2008 to 00-00-2008**

4. TITLE AND SUBTITLE	5a. CONTRACT NUMBER
Computational Study of Environmental Effects in the Adsorption of DMMP, Sarin, and VX on γ-Al2O3: Photolysis and Surface Hydroxylation	5b. GRANT NUMBER
	5c. PROGRAM ELEMENT NUMBER
6. AUTHOR(S)	5d. PROJECT NUMBER
	5e. TASK NUMBER
	5f. WORK UNIT NUMBER
7. PERFORMING ORGANIZATION NAME(S) AND ADDRESS(ES) **Naval Research Laboratory,4555 Overlook Avenue SW,Washington,DC,20375**	8. PERFORMING ORGANIZATION REPORT NUMBER
9. SPONSORING/MONITORING AGENCY NAME(S) AND ADDRESS(ES)	10. SPONSOR/MONITOR'S ACRONYM(S)
	11. SPONSOR/MONITOR'S REPORT NUMBER(S)

12. DISTRIBUTION/AVAILABILITY STATEMENT
Approved for public release; distribution unlimited

13. SUPPLEMENTARY NOTES

14. ABSTRACT

15. SUBJECT TERMS

16. SECURITY CLASSIFICATION OF:			17. LIMITATION OF ABSTRACT	18. NUMBER OF PAGES	19a. NAME OF RESPONSIBLE PERSON
a. REPORT **unclassified**	b. ABSTRACT **unclassified**	c. THIS PAGE **unclassified**	**Same as Report (SAR)**	**14**	

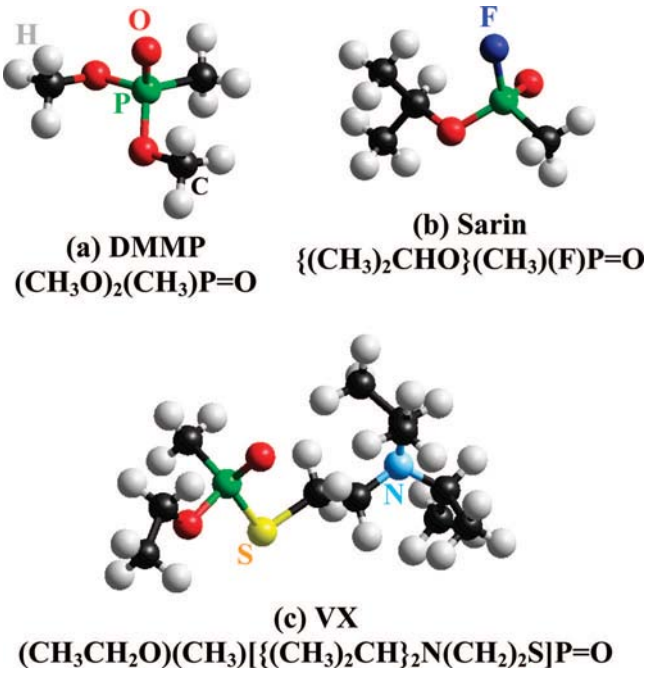

Figure 1. Schematic diagrams of the relevant molecular structures shown in the optimized gas-phase conformations (see text). The Sarin and VX enantiomers were arbitrarily chosen.

After a description of the computational details and a brief review of the relevant experimental data, attention will focus on the development and testing of the cluster models for the hydroxylated γ-Al_2O_3 surface. Next, a comparison of adsorption on the hydroxylated vs the OH-free surface will be presented, followed by an examination of photoexcitation in the gas- and adsorbed phases.

2. Computational Methods

Density functional theory (DFT) calculations were carried out using the Amsterdam density functional (*ADF 2006* or *2007*) code.[33] An advantage of this facility is the availability of pseudohydrogen (PH) atoms which are hypothetical neutral species having a noninteger nuclear charge and electron occupancy. As described elsewhere,[34,35] these are useful for terminating the coordinatively unsaturated atoms at the edges of free-standing ionic clusters. Passivating the highly reactive edge sites makes it possible to study the interaction of large and complex molecules such as VX with small clusters without incurring spurious bond formation (see below). Pseudo-H termination (PHT) also removes electronic states, due to unsaturated edge atoms, in the "band gap" of the cluster, i.e., the gap between the highest occupied molecular orbital (HOMO) and the lowest unoccupied molecular orbital (LUMO). This makes it possible to treat problems related to electronic excitation of adsorbed species.

The basis sets, designated "TZP", were Slater-type functions of triple-ζ quality with a single polarization shell added, i.e., a p shell for H and a d shell for all other atoms. These are all-electron basis sets with no "frozen cores" (cf. ref 33). The density functional consisted of the Vosko−Wilk−Nusair (VWN) form of the local density approximation (LDA) and the Perdew−Burke−Ernzerhoff (PBE) form of the generalized gradient approximation (GGA) exchange-correlation (XC) potential. The PBE formulation of the GGA−XC potential was used because it is compatible with analytical energy gradients in ADF and because it has previously been used[36−38] in DFT treatments of γ-Al_2O_3 bulk and surface properties.

For free molecules and for adsorption on the small cluster (see below) the convergence criteria in geometry optimization were 1×10^{-6} Hartree for total energy, 1×10^{-3} Hartree/Å for gradients, and 1×10^{-3} Å for displacements. The integration precision parameter was set at 7.0 (tighter than the default of 5.0), and it was verified that a higher value (8.0) had no significant effect. For adsorption on the large cluster, which was computationally demanding, it was necessary to relax the criteria to the default settings (1×10^{-3} Hartree for total energy, 1×10^{-2} Hartree/Å for gradients, 1×10^{-2} Å for displacements). Further details regarding geometry optimization are given below. The adsorption energy (ΔE_{ads}) is defined in the usual manner as

$$\Delta E_{ads} = E(\text{cluster} + \text{mol}) - E(\text{cluster}) - E(\text{mol}) + \Delta E(\text{BSSE})$$

where the E's are respectively the relaxed total energies of the cluster with the adsorbed molecule, of the bare cluster and of the free molecule. ΔE(BSSE) is a counterpoise correction for basis set superposition error (BSSE) which is applied except where noted. $\Delta E_{ads} < 0$ indicates an exothermic reaction.

Hydrogen bonding (H-bonding), including C−H···O bonds between alkyl groups and O atoms in the Al_2O_3 lattice, was analyzed using the Atoms in Molecules (AIM) approach[39] developed by Bader.[40] Critical points in the total electron density were located using the XAIM code.[41] The vibrational frequencies reported here are the purely harmonic values with no scaling correction. The appropriate scaling factor in the present case is thought to be close to unity.[42] The main interest is in small shifts in frequency caused by adsorption rather than in absolute frequencies; hence, scaling should be relatively unimportant. Furthermore, only the mid-IR-active internal modes of the adsorbed species are of interest here. Examination of the atomic displacements in each of these modes indicates that, in most cases, there is little or no contribution from motion of atoms in the Al_2O_3 cluster itself. Hence, the frequency results are reliable even though only partial optimization of the cluster geometry is performed (see below).

It is known[43] that proper description of excited electronic states requires the inclusion of diffuse functions in the basis sets. In the present case, QZ3P+1 basis sets and time-dependent density functional theory (TDDFT) were employed when treating electronic excitation. These basis sets are of quadruple-ζ quality with three polarization and one diffuse function added. The TDDFT studies were done as single-point calculations for structures optimized using time-independent DFT and TZP basis sets. The XC potential used in TDDFT was based on the statistical averaging of orbital potentials (SAOP) method[44] which has the correct $-1/r$ dependence for $r \rightarrow \infty$. Tests were done to verify that the computed excitation energies are independent of the technical aspects of the TDDFT calculation (e.g., integration accuracy, SCF convergence criteria, etc.). For studying the near-UV spectra of adsorbed species, QZ3P+1 basis sets were used for the molecule and for the Al(−O−)$_3$ site at which adsorption occurs (see below). In order to reduce the computational time, TZP basis sets were used for the rest of the cluster. No significant difference was seen when the Al(−O−)$_3$ adsorption site was also treated with TZP basis sets. Some TDDFT calculations were also done for free molecules using the *Gaussian 03* code[45] with the B3LYP functional and 6-311^{++}G(d,p) basis sets. These used "Tight" convergence criteria in geometry optimizations (with time-independent DFT) and an "UltraFine" integration grid.

3. Experimental Background

This section briefly summarizes the relevant experimental data for DMMP, Sarin, and VX both free and adsorbed on γ-Al_2O_3 and for the photochemical properties in the near-UV.

3.1. Free Molecules. The conformations of gas-phase DMMP and Sarin have been studied both experimentally[12,27] (using microwave spectroscopy) and theoretically.[4,10,12,27,46,47] Gas-phase vibrational spectra (which differ somewhat from those for the liquid) have been reported for DMMP (refs 48−50) and Sarin (ref 51); see also ref 23. During geometry optimization, here as before,[23−25] DMMP and Sarin relaxed into their lowest-energy conformations (Figure 1) which concur with those reported previously.[10,27] For Sarin, calculations of the relaxed total energy vs the angle of rotation of the $(CH_3)_2(H)C-$ group about the C-OP bond were done in 10° steps. The results (not shown) were very similar to those obtained previously[10] at the B3LYP/6-31G(d,p) level. In Sarin and VX, the P atom is an optically active center. In either case, only one arbitrarily chosen enantiomer (that shown in Figure 1) was considered here.

Rotational isomerization in VX and related species has been studied in dilute solutions using IR spectroscopy[52,53] and semiempirical theory.[53] The only isomerization detected involves hindered rotation about the CH_3CH_2O-P bond. However, VX in solution assumes a more compact geometry than in the vapor phase, for which other forms of isomerization may be possible. Rotational isomerization in isolated VX is discussed in more detail below and in the Supporting Information in connection with steric effects in adsorption. An ab initio computational study[1] for vapor-phase VX led to the optimized structure shown in Figure 1c. A similar study, at the B3LYP/6-31$^+$G(d) level, has been reported[7] for an analog of VX (termed "VX-Me") in which the ethoxy group is replaced by a methoxy and the isopropyl groups by methyl groups. Although different enantiomers were considered in the two studies, comparison of the torsion (dihedral) angles shows that the optimized structures are similar. Vibrational spectra are available[54−56] for VX with, in the case of Raman data,[56] detailed mode assignments.

3.2. Adsorption on γ-Al_2O_3. The interaction of DMMP with high-surface-area (HSA) γ-Al_2O_3 powder has been studied by Mitchell et al.[57] Results have also been reported for adsorption on an unspecified form of Al_2O_3 HSA powder,[58] on oxide layers on polycrystalline Al films[59] (believed to be γ-Al_2O_3), and on an oxide layer on an Al(111) surface.[60] For OH-free surfaces at room temperature, a nondissociative dative-bonding interaction[57,59] occurs between the coordinatively unsaturated tetrahedral Al(T_d) Lewis acid site and the O atom of the P═O group. Surface OH, if present, may also be involved through H-bonding to the P═O group and/or to an $-OCH_3$ group. Higher temperature promotes a nucleophilic attack by the O atom of an OH site on the P atom, causing the release of CH_3OH and the formation of a bridging structure. For nondissociative adsorption[57a,59a] only the ν(P═O) mode, at 1216 cm^{-1}, exhibits a substantial shift from the gas-phase value[48−50] (1276 cm^{-1}). Other modes appear at energies close to the gas-phase values. Reaction with OH affects modes related to the CH_3O- groups and further increases the red-shift in ν(P═O). At still higher temperatures[59] loss of the second CH_3O occurs with formation of an $(-Al-O-)_3PCH_3$ surface species. None of the data show any clear indication of shifts in the ν(O−H) modes of surface hydroxyls due to H-bonding to DMMP. However, such bonding is known[61] to result in a very broad ν(O−H) band which can be difficult to detect.

The adsorption of Sarin on HSA γ-Al_2O_3 powder has been studied experimentally using IR spectroscopy.[62,63] Initial adsorption occurs *via* a strong Al···O═P interaction which, on an hydroxylated surface, is followed by H_2O elimination, transfer of F to an adjacent Al site, and formation of a bridging structure analogous to that described above for DMMP. For nondissociative adsorption the IR data show, as the only major effect, a shift of $\Delta\nu$(P═O) = −63 cm^{-1} relative to the gas-phase value[51] of 1308 cm^{-1}. As in the case of DMMP, subsequent reaction with OH groups leads to more substantial changes in the IR spectra.

Experimental data for VX adsorption on Al_2O_3 are provided in the NMR studies of Wagner et al.[64,65] which involve the use of both aerogel-prepared Al_2O_3 nanoparticles and γ-Al_2O_3 HSA powders. For high VX loading, complete reaction of the entire nanoparticle occurs to form an aluminophosphonate complex. There is also evidence that H_2O and/or OH on the HSA powder promotes reaction with VX leading to a bidentate phosphonate structure.

3.3. UV Spectra and Photochemical Properties. A substantial amount of work has been done on the photocatalytic destruction of DMMP using TiO_2 and other metal oxides (see, e.g., refs 66 and 67 and works cited). These photoeffects are initiated by the excitation of electron−hole pairs in the oxide. In the present work, we are concerned with the photoexcitation of CWAs themselves when adsorbed on a photochemically inert oxide. With a bulk band gap of ∼7.2 eV (ref 68), γ-Al_2O_3 is transparent throughout the photochemically active part of the terrestrial solar spectrum[69] (TSS), the intensity of which is negligible above about 4.5 eV (see below).

The UV spectra of DMMP and Sarin, in the vapor phase or dissolved in cyclohexane or ethanol, have been reported.[70−72] Both are weak absorbers at wavelengths longer than ∼200 nm (energies below ∼6.2 eV). In cyclohexane,[70] DMMP shows a weak band (possibly due to an impurity) at 205 nm (6.1 eV), and in the vapor phase[71] there appears to be a stronger band (or shoulder) at ∼160 nm (7.8 eV). This shoulder lies on the edge of what appears to be a strong absorption continuum. Sarin in the vapor phase shows no absorption for $\lambda > 200$ nm but in ethanol exhibits a weak band at about 204 nm which may be due to an impurity.[72] Aschmann et al.[73] observed no significant photochemical decomposition of gas-phase DMMP during irradiation at $\lambda > 300$ nm ($h\nu < 4.1$ eV). Rauk et al.[15] have calculated the lower-lying electronic transitions of a Sarin analog with CH_3 replacing $(CH_3)_2CH$. At the MP2/6-31$^+$G(d) level the excitation threshold is found at about 9.9 eV, somewhat higher than that computed here for Sarin (see below).

VX dissolved in cyclohexane was found[70] to be a somewhat stronger UV absorber than DMMP or Sarin; although, no actual absorption peaks were seen for $\lambda > 200$ nm. Zuo et al.[74] studied VX dissolved in ethanol and found absorption maxima at 209, 238, and 266 nm (5.93, 5.21, and 4.66 eV). These were analyzed (for the gas-phase molecule) at the restricted Hartree−Fock (RHF) level using the configuration interaction singles[43] approach with STO-3G basis sets. Irradiation of VX droplets in air at 253.7 nm (4.89 eV) led to a complex series of molecular rearrangements and also to reaction with photogenerated ozone. The reported UV spectra[70,74] for VX differ qualitatively; although, the effect of the solvent (cyclohexane vs ethanol) is uncertain.

4. Construction of γ-Al_2O_3 Surface Models

This section describes the construction and evaluation of the cluster models for the hydroxylated surface. It will be shown that the models give a good description of both the chemical and the electronic structure of the hydroxylated γ-Al_2O_3 surface

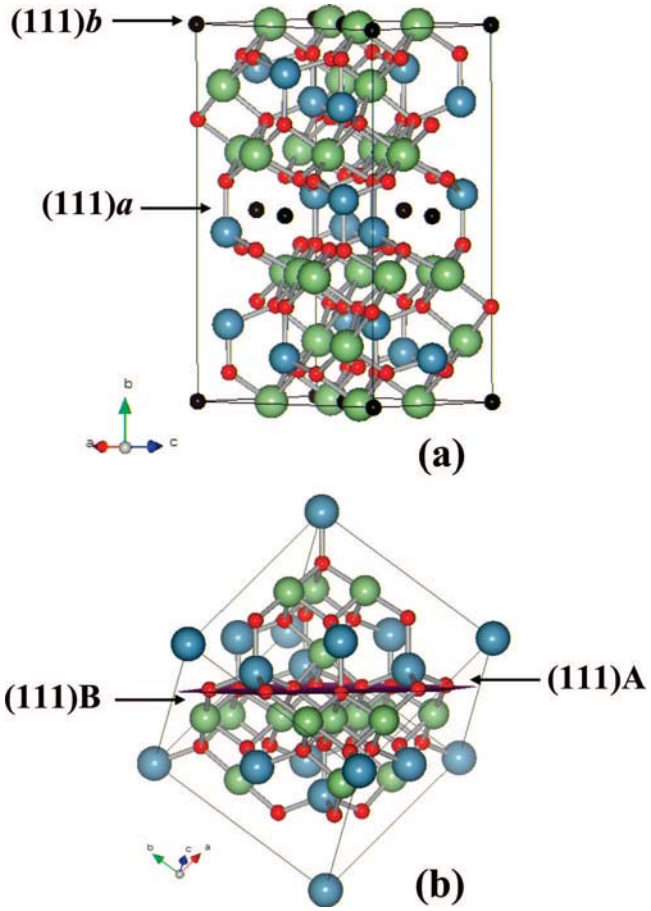

Figure 2. Models for (a) the defective-spinel and (b) the ideal spinel γ-Al_2O_3 lattices. Blue, green, and red spheres are respectively Al(T_d), Al(O_h), and O. In (a) the small black spheres represent Al(O_h) vacancies. Different surface planes are identified.

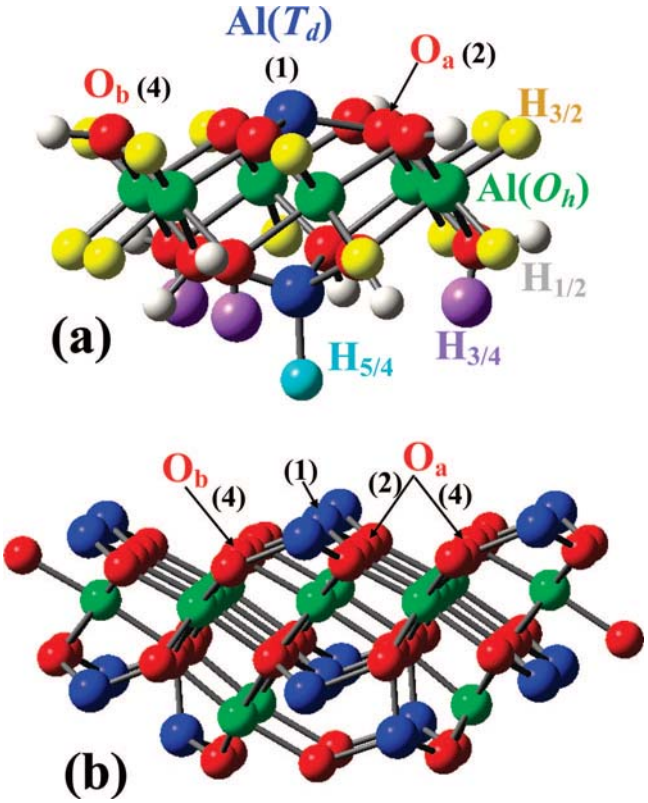

Figure 3. Models (not to scale) for the (a) Al_8O_{12} and (b) $Al_{32}O_{48}$ clusters. For clarity, the pseudo-H atoms ($H_{1/2}$, etc.) are shown only for (a). Examples of the different O-atom types (O_a and O_b) are labeled. At the "surface", an O_a is bonded to two Al(O_h) and one Al(T_d), and an O_b is bonded to three Al(O_h). The "1" labels the central Al(T_d) site, and "2" and "4" label atoms according to their distance from this site. Site "3" would be a subsurface Al(O_h). Thus placing an OH on the central Al and H on the nearest O_b gives a 1,4 configuration.

and that there is no pronounced dependence of the properties of the OH groups on the size of the PH-terminated clusters. These results are general and will be useful in other studies of the hydroxylated γ-Al_2O_3 surface.

4.1. OH-Free Surface. The bulk and surface structures of γ-Al_2O_3 are controversial and are discussed briefly in refs 23 and 25 together with a description of cluster models for the OH-free surface. The controversy centers on whether a defective-spinel or a nonspinel model is more appropriate, and a recent study[75] (which reviews earlier work) suggests that γ-Al_2O_3 should actually be seen as an amorphous random network of Al−O bonds. The model for the bulk structure determines the structure and stability of the different surface planes which, in turn, influences the identity and the distribution of reactive surface sites (both OH-free and hydroxylated).

In the present work, as before, the point of departure is the defective-spinel model for bulk γ-Al_2O_3 described by Pinto et al.[76,77] and shown[78] in Figure 2a. Further details are given in the Supporting Information. Following convention, the γ-Al_2O_3 surface planes are labeled according to the corresponding planes of the spinel lattice from which they are derived. Thus the (010) plane of the monoclinic defective-spinel unit cell in Figure 2a corresponds to the (111) plane of the cubic spinel lattice, Figure 2b. The most stable surface in this model (the (111)*a* in the spinel labeling) is formed by "cleaving" on the layer of vacancies shown in Figure 2a. This surface consists of singly unsaturated tetrahedral Al(T_d) sites and two types of O sites. One site (termed "O_a" in the present work) is 3-fold coordinated in the bulk, as a result of being adjacent to a vacant octahedral Al(O_h) site, and remains so at the surface. An O_a has one Al(T_d) and two Al(O_h) nearest-neighbors. The other O site (termed "O_b") is 4-fold coordinated in the bulk but is missing its Al(T_d) nearest-neighbor at the surface and thus has three Al(O_h) nearest-neighbors. There are no unsaturated Al(O_h) sites on the (111)*a* surface.

Figure 3 shows two clusters cut from the (111)*a* surface shown in Figure 2a. These are of stoichiometry Al_8O_{12} and $Al_{32}O_{48}$ and are used with PHT as described in the Supporting Information. In both cases, the reactive cation surface site, in the absence of OH, is an Al(T_d) which is known from experiment[57,59,62] to be important in the adsorption of DMMP and Sarin. In the first step in geometry optimization for OH-free surfaces, the Al and O atoms in the cluster were frozen in the ideal bulk-lattice positions while the PHs were all allowed to vary. In subsequent optimizations, most of the PH, Al, and O atoms remained fixed (see below).

4.2. Hydroxylated Surface. ***4.2.1. Chemical Structure.*** The structure of the hydroxylated γ-Al_2O_3 surface is complex and not yet fully understood. Many chemically distinct OH sites are possible, depending on the surface structure and treatment. Empirical models have been proposed,[79−83] based on analyses of the IR spectra of HSA powders and the response to chemical treatment, which correlate the ν(O−H) stretching frequency with the structure of the OH site. Recently these models have been further investigated using quantum-chemical methods.[84−86] The general consensus is that ν(O−H) falls in approximately the 3760−3800 cm^{-1} range for type I sites (OH bonded to a single surface Al), 3700−3750 cm^{-1} for type II sites (OH bridging

two Al's), and 3635−3700 cm^{-1} for type III sites (OH bonded to three Al's). For each type of site, various combinations of Al(O_h) and Al(T_d) are possible. For example, a type II OH bridging two Al(O_h) sites is chemically distinct from one bridging an Al(O_h) and an Al(T_d).

The (111)*a* surface described above differs from both the (111)A and (111)B surfaces typically invoked in discussions[79,82] of the spinel-like γ-Al_2O_3 lattice. Figure 2b shows the ideal-spinel γ-Al_2O_3 lattice which involves no Al vacancies and is therefore nonstoichiometric (see Supporting Information). Cleaving on the plane indicated generates the (111)A and (111)B surfaces. When fully reacted with H_2O, the former exhibits type I Al(T_d)−OH and type II Al(O_h)−O(H)−Al(T_d) sites in a 1:3 ratio. The latter involves type II Al(O_h)−O(H)−Al(O_h) and type III [Al(O_h)]$_3$−OH sites in a 3:1 ratio. These points are discussed more fully in refs 79 and 82. When the optimal distribution of Al(O_h) vacancies is considered in the defective-spinel model,[76,77] the (111)*a* plane shown in Figure 2a becomes the lowest-energy surface since it cuts through a high density of vacancies. On this surface, a type I Al(T_d)−OH site and type-III [Al(O_h)]$_2$[Al(T_d)]−O_aH or [Al(O_h)]$_3$−O_bH sites are formed. Henceforth, these type III sites will be termed "type IIIa" and "type IIIb. Two-dimensionally periodic slab (2-DPS) calculations[77] for the dissociative adsorption of H_2O show little dependence of ΔE_{ads} (at most ∼5%) on which O site is chosen for the H atom (see below).

In order to construct a viable computational model for adsorption on the hydroxylated surface, one which can be compared with data for HSA powders, it is necessary to determine which OH sites are important. For DMMP, Mitchell et al.[57a] found that the OH sites removed in the initial adsorption at room temperature correspond to a loss of intensity in the range of ∼3700−3750 cm^{-1}. Similar data have been reported[59] for DMMP adsorption on Al_2O_3 films on polycrystalline Al. These were thought to be of the γ form and free of physisorbed H_2O. Here adsorption led to a loss of intensity in the 3630−3650 cm^{-1} range. For Sarin the reactive OH group corresponds[62] to a ν(O−H) of 3700 cm^{-1}. These results all exclude type I sites as the active species, but type II and type III remain as possibilities. Type I sites may be present as spectators but, in view of the IR data, they do not participate in the initial adsorption of DMMP or Sarin.

The models in Figure 3 were hydroxylated by dissociatively adsorbing H_2O (see below). An OH was placed at the center of the surface, to form a type I Al(T_d)−OH, and an H at either an O_a or O_b site to form a type IIIa or IIIb OH site. The discussion thus far has been entirely in terms of the defective-spinel model for γ-Al_2O_3. Examining the nonspinel model[84] one finds that type IIIb sites also form on the (100) and (111) surfaces and that this is the only type III site (termed "HO-μ_3-Al_{VI}" in ref 84) on the low-index surfaces of this model. The type I Al(T_d)−OH (termed "HO-μ_1-Al_{IV}" in ref 84) is also found on the (110) nonspinel surface. Hence the results obtained here should be generally applicable to both γ-Al_2O_3 models. The OH sites treated here consist of the basic type I and the acidic type III, and it is found that OH···O═P bonding clearly favors the latter (see below). This limiting behavior then provides a firm basis for estimating (in lieu of actual results) the behavior of intermediate sites such as the type II found on other surfaces of both the spinel and nonspinel models. Likewise, the present models consider only the Al(T_d) site on the OH-free surface. The nonspinel model[84b] also involves unsaturated Al(O_h) surface sites, but these are found to be lower in Lewis-acidity and are thus expected[25] to be less active in dative bonding to the P═O group.

Geometry optimization was performed for the hydroxylated models. These were partial optimizations which included all Al atoms in the "surface" (one for Al_8O_{12} and seven for $Al_{32}O_{48}$), the three O nearest-neighbors of the type I Al(T_d)−OH and the O_a or O_b atom to which the H was added. The adsorbed H and OH were also included in the optimization. The rest of the Al and O atoms remained fixed in the bulk-lattice positions, and the PHs were frozen in the previously determined optimized positions.

4.2.2. Formation via Dissociative Adsorption of H_2O. This section examines ΔE_{ads} for the chemisorption of H_2O on the OH-free surface which is a useful quantitative test. The energetics of the process whereby the OH-free cluster is converted to the proposed model hydroxylated surface should be consistent with results for the chemisorption of H_2O. The related issue of the physisorption of molecular H_2O, in comparison to 2-DPS results, is discussed elsewhere[25] as a quantitative test of the OH-free model surface.

Previous 2-DPS results[77] for dissociative adsorption of H_2O on the (111)*a* surface showed little dependence of ΔE_{ads} on the placement of the H atom, relative to the type I Al(T_d) site, or on whether a type IIIa or IIIb site was formed. A ΔE_{ads} of −36.2 to −38.0 kcal/mol was found for all of the configurations considered. In the present work, 2-DPS calculations[25] were done for dissociative adsorption in a 1,4 configuration with H at a type IIIb site and in a 1,2 configuration with H at a type IIIa. After correction for BSSE, the former gave ΔE_{ads} = −33.9 kcal/mol, and the latter gave −34.9 kcal/mol. In this notation "1" refers to the Al site with the type I OH group, and "2" or "4" refers to placement of the H atom on a first- or third-nearest-neighbor O atom. The second-nearest-neighbor of an Al(T_d) is an Al(O_h); hence, no 1,3 OH configuration is formed. These results will now be compared with those for the clusters.

For the Al_8O_{12} cluster (Figure 3a), an OH is placed on the Al(T_d) site and an H on the O_b atom in a 1,4 configuration. The latter is a type IIIb site if the $H_{1/2}$ PH is counted as the third Al(O_h) neighbor. This is justified in that the properties of this site (see below) compare well with those of a 1,4 type IIIb site on the larger $Al_{32}O_{48}$ cluster. This structure gave ΔE_{ads} = −33.8 kcal/mol which compares well with the present 2-DPS result (−33.9 kcal/mol). Hence, even the small Al_8O_{12} cluster, with PHT, can give good results for the chemisorption of H_2O. However, placing the H on the O_a site gives a 1,2 configuration with ΔE_{ads} = −29.9 kcal/mol which differs somewhat from the present 2-DPS result (−34.9 kcal/mol).

Similar calculations were done for the $Al_{32}O_{48}$ cluster (Figure 3b). The 1,4 configuration with H on an O_b site gave ΔE_{ads} = −37.3 kcal/mol which is fairly close to the 2-DPS result (−33.9 kcal/mol). The optimized type III O_b−H_{ads} distance was 0.978 Å. For the type I Al−OH, the Al−O and O−H distances were 1.758 and 0.971 Å, respectively, and the Al−O−H bond angle was 112°. The larger $Al_{32}O_{48}$ cluster allows more flexibility in the choice of the site for the H atom. Another 1,4 configuration, but one involving an O_a site, gave ΔE_{ads} = −28.9 kcal/mol which again differs somewhat from the 2-DPS result. This result is, however, close to the value (−29.9 kcal/mol) obtained above for a 1,2 type IIIa configuration on the Al_8O_{12} cluster.

To summarize the cluster results, the 1,2 and 1,4 type IIIa structures give very similar energies, whereas 1,4 type IIIa and 1,4 type IIIb configurations give somewhat different values with the latter being in better agreement with 2-DPS results. Thus,

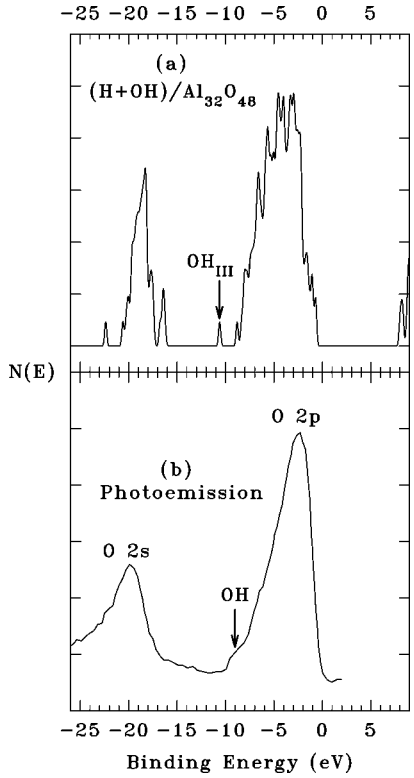

Figure 4. (a) Computed DOS for the hydroxylated $Al_{32}O_{48}$ cluster shown in Figure 3b. The zero of energy is the VBM. A bonding state derived from the type-IIIb OH site is indicated. The DOS has been broadened with an arbitrarily chosen Gaussian width of 0.27 eV. (b) SXPS data (ref 87 with permission) for an hydroxylated Al_2O_3 film on Al (110). The energy scale has been shifted by 1.0 eV from that given in the original reference to place the VBM at the foot of the strong peak so as to be consistent with (a). The feature assigned in ref 87 to OH is marked. "O 2s" and "O 2p" indicate the dominant orbital composition of the two SXPS bands.

ΔE_{ads} is nearly independent of the distance between the type I and III sites, in agreement with the 2-DPS models, but there is a dependence on whether a type IIIa or IIIb site is formed which is not seen for the 2-DPS.

4.2.3. Surface Electronic Structure. The discussion thus far has focused on the accuracy of the cluster model with respect to surface-chemical properties. Another test is based on the electronic structure. In the following, reference will be made to the "valence band" (VB) of the cluster and to the "valence band maximum" (VBM), neglecting the fact that the cluster orbitals constitute a finite (albeit closely spaced) set of discrete states. Soft-X-ray photoemission spectroscopy (SXPS) data[87] for hydroxylated Al_2O_3 films on an Al (110) surface (Figure 4b) show a bonding state, for an unknown type of OH site, at about 9 eV below the VBM. Figure 4a shows the density of states (DOS) computed for the 1,4 type IIIb configuration of the $Al_{32}O_{48}$ cluster (Figure 3b). A deep-lying state, due to the type IIIb OH site, is seen at 10.6 eV below the VBM. Results (not shown) for the 1,4 type IIIa configuration are similar, with the type IIIa OH feature at 8.8 eV below the VBM. For the 1,4-hydroxylated Al_8O_{12} cluster the type IIIb OH peak falls at 9.1 eV below the VBM.

To investigate this issue further, DOS results (not shown) were obtained for the present 2-DPS calculations. These gave a type IIIb OH peak at 9.6 eV below the VBM in good agreement with experiment and with the cluster calculations. The type I OH gave a broad peak, centered at ∼5.8 eV below the VBM, due to the AlO−H bond and a narrower peak, just below the VBM, due to the Al−OH bond. For the $Al_{32}O_{48}$ (Al_8O_{12}) cluster the corresponding type I states lie at ∼5.9 (5.4) and 1.2 (1.0) eV below the VBM. The type I OH features are not readily observable in SXPS due to the strong emission from the Al_2O_3 VB; however, both clusters give DOS results in good agreement with the 2-DPS and with the available experimental data.

TABLE 1: Deprotonation Energies for the Hydroxylated Clusters[a]

OH type	Al_8O_{12}	$Al_{32}O_{48}$
I		(∼1600)[b]
IIIa	1228	1161
IIIb	1244	1199

[a] Energies are given in kJ/mol to conform with refs 88 and 89 and have been corrected for a vibrational zero-point energy of 30 kJ/mol associated with the O−H stretching and bending modes (see text). All values are positive (endothermic). The smaller the ΔE_{dp} the more acidic the OH group. Both clusters are pseudo-H terminated. [b] The deprotonated type I site is metastable (see text). This result is an estimate.

4.2.4. Brønsted Acidity. The acidity of the different OH types is important in reactivity. Nortier et al.[88] have estimated the Brønsted acidity of OH on δ- and θ-Al_2O_3 by computing the deprotonation energy (ΔE_{dp}) at the RHF level using small cluster models and effective-core pseudopotentials. For deprotonation of a species XOH, ΔE_{dp} is defined as $E(XO^-) + E(H^+) - E(XOH)$ where XO^- and H^+ are at infinite separation and experience no Coulombic attraction. ΔE_{dp} is positive (endothermic) and decreases with increasing acidity. For Al_2O_3, ΔE_{dp} decreases in the order type I > type II > type III. The type IIIa site is found[88] to be the most acidic, more so than the type IIIb. The type I Al(T_d)−OH exhibits the second-lowest acidity, with only the type I Al(O_h)−OH site being the less acidic. A similar ordering of acidities was also obtained in another study[89] of small clusters at the RHF/3-21G level.

Deprotonation energies (Table 1) were obtained here using the DFT methods and hydroxylated clusters described above. These have not been corrected for BSSE, but based on results obtained above, including ΔE (BSSE) would reduce all ΔE_{dp} values by only ∼5 kJ/mol. A correction has been applied for the zero-point energies of the O−H stretching and bending modes which are lost upon deprotonation. This reduces the purely electronic ΔE_{dp} by ∼30 kJ/mol. The ordering of acidities in Table 1 agrees with that in previous work; although, the difference between type IIIa and IIIb sites is not as large. Also, the Al_8O_{12} results, although larger than the corresponding $Al_{32}O_{48}$ values, are reasonably close to those for the larger cluster.

The calculations differ somewhat from those of Nortier et al.[88] in that two types of OH sites are present when one or the other is deprotonated. For example, when deprotonating a type I OH there is also a nearby type III OH which retains its proton. This situation is more relevant to the present investigation than is an isolated OH. It was found here that the deprotonated type I site is metastable on either cluster. Relaxation leads, ultimately, to migration of the H atom from the type IIIb site to the Al(T_d)−O^- to reform the type I OH at the expense of the type IIIb. This is a clear indication of the lower type I OH acidity since the deprotonated type I site lies higher in energy than the deprotonated type III. An estimate of $\Delta E_{dp} \approx 1600$ kJ/mol for the type I OH is obtained from the energy of the metastable configuration formed after the initial large relaxation but before the start of pronounced H-atom migration.

TABLE 2: Structural and Energetic Results for Nondissociative Adsorption of DMMP, Sarin, and VX on PH-Terminated Clusters[a]

cluster	adsorbate	ΔE_{ads}	r(Al−OP)	r(AlO=P) [b]	∠(Al−O=P)	$\Delta\nu(P=O)$
Al_8O_{12} (OH-free)	DMMP	−53.0	1.819	1.523 (1.490)	149	−62[c]
	Sarin	−51.5	1.838	1.521 (1.481)	132	−103[d]
	VX	−51.6	1.814	1.537 (1.497)	137	−95[e]
$Al_{32}O_{48}$ (OH-free)	DMMP	−41.4	1.860	1.516	148	
	Sarin	−39.8	1.863	1.513	130	
	VX	−39.3	1.860	1.534	136	

[a] In all cases, adsorption is via Al(T_d)···O=P dative bond formation. Energies are in kcal/mol, bond lengths in Ångstroms, bond angles in degrees and frequencies in cm^{-1}. The $\Delta\nu$(P=O) values are based on the harmonic values with no scaling correction. $\Delta\nu$(P=O) is ν(P=O) calculated for the adsorbed species minus that calculated for the gas-phase. The DMMP and Sarin results repeat those in ref 25. All energies are BSSE-corrected. [b] Numbers in parentheses are the P=O bond lengths computed for the free molecules. [c] The experimental result is −60 cm^{-1} (ref 57), based on a gas-phase ν(P=O) of 1276 cm^{-1} (refs 48−50). For adsorbed DMMP the computed P=O stretch is strongly coupled to modes at 1161 and 1174 cm^{-1}, and ν(P=O) is taken as the average. [d] The experimental result is −63 cm^{-1} (ref 62), based on a gas-phase ν(P=O) of 1308 cm^{-1} (ref 51). [e] No corresponding experimental data are available.

5. Results and Discussion

5.1. Adsorption on OH-Free Surfaces. The adsorption energies and geometries for DMMP and Sarin on OH-free γ-Al_2O_3, computed using PH-terminated clusters, are given elsewhere[25] and are repeated in Table 2 together with new results for VX. The dependence of ΔE_{ads} on cluster size and on adsorbate has been discussed[25] in terms of the energy difference between the donor level of the free molecule and the acceptor level associated with surface Al(T_d) site. For the defective-spinel model[76,77] for γ-Al_2O_3, the Lewis acidity of the Al(T_d) site is better represented by the $Al_{32}O_{48}$ cluster, whereas the Al_8O_{12} overestimates the acidity and, therefore, ΔE_{ads}. On the other hand, the Al_8O_{12} cluster gives a better description of the Lewis acidity (and thus of ΔE_{ads}) for the Al(T_d) site on the surface of the nonspinel model.[84] The unpassivated $Al_{20}O_{30}$ cluster[23] (i.e., with no PHT) significantly overestimates the Al(T_d) Lewis acidity, and therefore the absolute ΔE_{ads} values.[25] However, relative ΔE_{ads} values as well as adsorption geometries and trends in ΔE_{ads} for different bonding configurations are essentially independent of the cluster.

For DMMP and Sarin, adsorption via dative bond formation between the phosphonyl O atom and the Al(T_d) is energetically favored over other bonding modes. For example, adsorption of Sarin on the Al_8O_{12} cluster via bond formation between Al(T_d) and the F or the isopropoxy O atom gives ΔE_{ads} = −26.2 and −31.0 kcal/mol, respectively. These have not been corrected for BSSE, and doing so would decrease the magnitude of ΔE_{ads} by about 2 kcal/mol. Both are already much smaller than the BSSE-corrected value of −51.5 kcal/mol (Table 2) for adsorption *via* an Al···O=P bond. The VX results are discussed in more detail below. Table 2 also gives results for $\Delta\nu$(P=O) computed for the smaller cluster. A similar analysis for the larger cluster is not computationally feasible at present. For DMMP, the purely harmonic values are in good agreement with the experimental result[57a,59a] of −60 cm^{-1}. For Sarin on the other hand, the computed $\Delta\nu$(P=O) of −103 cm^{-1} differs significantly from the experimental value[51,62] of −63 cm^{-1}. This discrepancy has been discussed previously.[25]

The effect of the adsorbate on the cluster has also been considered. For the bare Al_8O_{12} cluster, with all atoms initially in bulk-lattice positions, relaxation of the Al(-O-)$_3$ adsorption site results in an inward displacement of δz = −0.26 Å for the Al(T_d) which compares well with the 2-DPS result[76] of −0.33 Å. Smaller displacements are found in both cases for the O atoms. Adsorption largely reverses this inward displacement. After adsorption of DMMP, for example, δz for the Al(T_d) is only −0.04 Å relative to the unrelaxed bare cluster. Thus, adsorption causes an outward displacement of about 0.22 Å relative to the relaxed bare cluster.

For VX, bonding between Al(T_d) and the O atom of the CH_3CH_2O- group is not considered here since this is already known, in the case of DMMP and Sarin, to be less favorable than bonding to the O atom of the P=O group. However, it is necessary to investigate adsorption via an Al···S or Al···N bond. The latter, in particular, might be strong at a Lewis-acid surface site. The use of the small Al_8O_{12} cluster reduces, as much as possible, the importance of steric factors and of multiple bonding interactions (see below). This enables an unbiased evaluation of the electronic contribution of just a single dative bond to the adsorption energies. The results (not corrected for BSSE) are ΔE_{ads} = −30.4 kcal/mol, r(Al−N) = 2.10 Å for Al···N and ΔE_{ads} = −34.8 kcal/mol, r(Al−S) = 2.38 Å for Al···S. These energies are significantly less than the corresponding BSSE-corrected value of −51.6 kcal/mol (Table 2) value for Al···O=P formation.

Figure 5 shows the three optimized VX structures. Passivation of unsaturated edge sites (accomplished here through the use of PHT) is essential in the case of a large, polyfunctional, and "flexible" molecule like VX. Results (not shown) for an unpassivated $Al_{20}O_{30}$ cluster indicated a tendency for the molecule to distort so as to allow an H atom in one of the isopropyl $-CH_3$ groups to interact with an Al edge site. With PHT, this spurious effect is not seen even for the smaller Al_8O_{12} cluster. When adsorbed on either cluster, all three species exhibited two or more CH···O bonds between alkyl H atoms and O atoms on the Al_2O_3 surface which were identified using AIM analysis. This form of H-bonding is commonly found in the adsorption of phosphonyl species on oxide surfaces.[19−22,26] The AIM results for the hydroxylated surfaces are discussed in more detail below.

5.2. Adsorption on Hydroxylated Surfaces. ***5.2.1. Al_8O_{12} Cluster.*** Experiment[57,59,62] suggests that Al−OH···O=P bonding (in addition to Al···O=P dative bonding) may be important when OH groups are present. The first set of calculations was done using the Al_8O_{12} cluster so that $\Delta\nu$(P=O) could be obtained and so that bonding to different types of OH groups could be studied individually while avoiding as much as possible any complications due to other forms of bonding.

5.2.1.1. DMMP. Results for the adsorption of DMMP will be analyzed in detail first, in order to make comparisons with experiment and to provide a framework for subsequent discussions of Sarin and VX, for which fewer experimental results are available. The surface was hydroxylated in the 1,2 or 1,4 configuration (Figure 3a), and a DMMP molecule was then

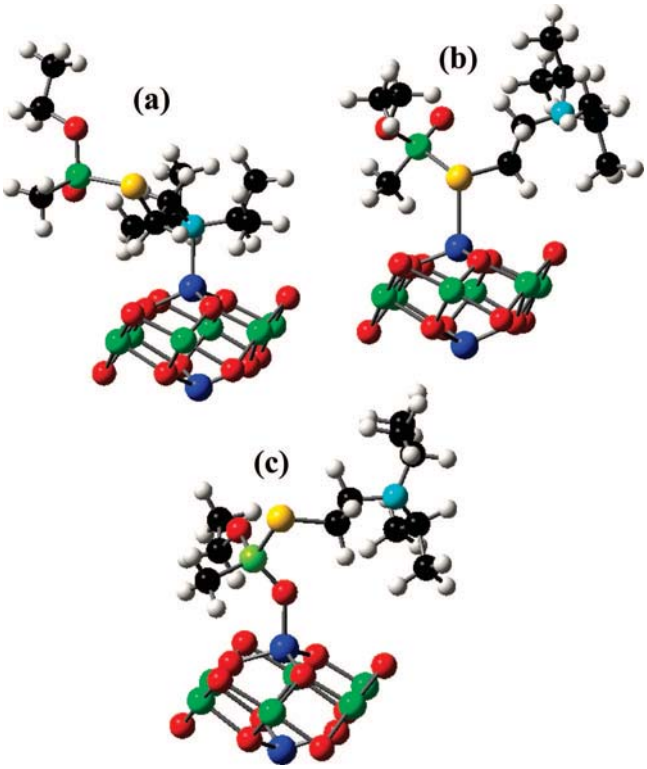

Figure 5. Optimized structures for bonding of VX to the Al_8O_{12} cluster (with PHT). Bonding is via (a) the N atom, (b) the S atom, and (c) the phosphonyl O atom. Configuration (c) is energetically favored (see text). For clarity the PHs are not shown.

positioned with the O atom of the P═O or P−O−CH_3 group oriented toward one OH or the other and the geometry optimized. The optimization procedure was the same as that described above for the hydroxylated surface but also included the DMMP. The resulting adsorption energies are given in Table 3, and some representative structures are shown in Figure 6. Most of the following discussion will focus on the type IIIb structure since, as noted above, this is more accurately described by the cluster models than is the type IIIa.

For the P═O group, $\Delta E_{ads} = -4.5$ and -23.2 kcal/mol were found for H-bonding to the type I and type IIIb site, respectively, with r(H···O) distances of 1.837 and 1.451 Å. Of the two, the type III is clearly more favorable which is consistent with its higher Brønsted acidity and with experimental results[57,59,62] showing that type I OH sites are not the primary sites for the initial adsorption of DMMP or Sarin. However, even the highest H-bond energy is smaller than ΔE_{ads} for Al(T_d)···O═P bonding to an OH-free cluster (Table 2). Thus the P═O group is favored both for H-bonding and for dative-bonding to the Al(T_d).

Figure 6 shows that, in addition to the main O−H···O═P bond, some of the methyl H atoms form C−H···O bonds. These were examined using the AIM approach, and some results are given in Table 4. The application of AIM specifically to C−H···O bonds has been discussed previously.[90−92] The C−H···O bonds found here all exhibit 3,−1 critical points[39,40] with a charge density (ρ) and a Laplacian of the charge density ($\nabla^2\rho$) in the range expected[90] for such bonds. The bond lengths and angles are also characteristic of C−H···O bonds.[90,93,94] It has been shown[90,95] that the bond energy between two species forming more than one H-bond is proportional to the total ρ at all H-bond critical points. On this basis, Table 4 shows that the O−H···O bond accounts for about 70% of ΔE_{ads}. The C−H···O bonding is, therefore, not sufficiently strong to have a significant effect on the comparison between ΔE_{ads} for different bonding configurations.

In order to check for basis-set dependence, some calculations were repeated using TZ2P basis sets. These differ from the TZP basis sets described above in the addition of a second polarization shell (d for H and f for all other elements). The calculations were done for adsorption via an OH···O═P bond at either the type I or type IIIb site. The calculations include the geometry optimization of the bare cluster, the free molecule and the cluster+molecule combination as well as the BSSE correction. The results, -3.7 and -24.3 kcal/mol respectively, are close to the corresponding TZP values of -4.5 and -23.2 kcal/mol given above.

Another check involved the choice of functional. Zhao and Truhlar[96] have designed a series of GGA XC functionals which, for H-bonding and noncovalent interactions, are often superior to those more commonly used (such as the PBE functional employed here). In *ADF 2007* these functionals can be applied a posteriori using the SCF density obtained in a PBE calculation. The M06−2X functional[96] was used to re-evaluate ΔE_{ads} for DMMP bonding via the P═O group to either the type I or type IIIb OH site (using TZP basis sets). The results (uncorrected for BSSE) were -5.7 and -29.6 kcal/mol, respectively, for M06−2X vs -5.1 and -24.5 kcal/mol for PBE (also uncorrected for BSSE). The results are not sufficiently different to affect the present analysis.

Vibrational frequencies were computed for DMMP adsorbed at the type IIIb OH site. A $\Delta\nu$(P═O) of -78 cm^{-1} was found, relative to the computed gas-phase value. This is a somewhat larger shift than is seen for adsorption via an Al(T_d)···O═P bond, either in experiment[57a,59a] (-60 cm^{-1}) or computationally (-62 cm^{-1}, Table 2). Apparently H-bonding can have a larger effect than dative bonding on ν(P═O), even though ΔE_{ads} is smaller. Bertilsson et al.[49] have reported IR data for DMMP adsorbed from the vapor phase onto alkanethiolate self-assembled monolayers (SAMs) terminated in −OH or −CO_2H tail groups. Adsorption occurs via an OH···O═P bond analogous to those studied here. For bonding to the acidic −CO_2H group, ν(P═O) was found at 1220 vs 1276 cm^{-1} in the gas phase, giving $\Delta\nu$(P═O) = -56 cm^{-1}. A room-temperature adsorption enthalpy of $\Delta H_a \approx 15.3$ kcal/mol (64.0 kJ/mol) was estimated by applying Brunauer−Emmett−Teller theory to adsorption measurements. Both $\Delta\nu$(P═O) and ΔH_a are smaller in magnitude for bonding to a terminal (alcoholic) OH group. A gas-phase thermochemical calculation performed here (see below) gave $\Delta H_a = 21.8$ kcal/mol for adsorption via an OH···O═P bond to the type IIIb site (adopting the sign convention of ref 49). As noted above, ∼70% of ΔE_{ads} for DMMP adsorption on the hydroxylated Al_8O_{12} cluster is derived from the OH···O═P bond. Reducing the ΔE_{ads} contribution to ΔH_a by 30% gives $\Delta H_a \approx 15.3$ kcal/mol which, perhaps fortuitously, is identical to the experimental estimate for bonding to the −CO_2H-terminated SAM.

The preceding discussion presents both theoretical and experimental evidence indicating that there is no simple, direct correlation between ΔE_{ads} and $\Delta\nu$(P═O) for the Al(T_d)···O═P dative bond. This observation has been made in a previous study[25] where a similar $\Delta\nu$(P═O) was computed for two species (Cl_3P═O and $(CH_3)_3$P═O) with very different ΔE_{ads} values. This appears to be a general result, suggesting that $\Delta\nu$(P═O) depends on other factors beyond just the bond energy. Understanding this effect will require further investigation.

The computed harmonic $\Delta\nu$(P═O) values are not sufficiently accurate that H-bonding can be ruled out in the experimental

TABLE 3: Adsorption Energies (ΔE_{ads}) for H-Bonding to the Al_8O_{12} Cluster[a]

	DMMP		Sarin			VX[b]			
OH type	P=***O***	P−***O***−Me	P=***O***	P−***O***−Me	P−***F***	P=***O***	P−***O***−Et	P−***S***−R	R′−***N***−(R″)$_2$
type I	−4.5	−5.0			−4.0	−2.4		+0.34[c]	−3.8
type IIIa	−13.7	−9.9							
type IIIb	−23.2	−13.9	−21.9	−10.4	−8.8	−19.0	−8.0	−10.1	(d)

[a] All energies are in kcal/mol and have been corrected for BSSE. The terms "type I", etc. are defined in the text. Missing entries are judged not to be relevant (see text) and have not been computed. The bold, italicized atom is the one to which the H-bond is formed. [b] R″ is a $-C(H)(CH_3)_2$ group; R′ is the $-CH_2CH_2-$ group; R is the $-R'N(R'')_2$ group. "Et" refers to the ethyl group. See Figure 1c. [c] Essentially no bonding occurs in this case. [d] Geometry optimization led to proton transfer from the OH to the N atom (see text).

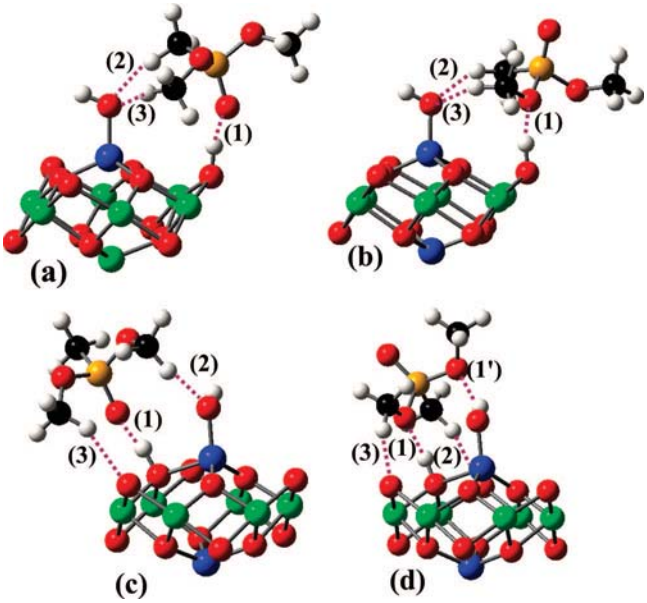

Figure 6. Optimized structures for DMMP adsorbed on the Al_8O_{12} cluster. (a) Bonding at the type IIIb site to the P=O group; (b) Bonding at the type IIIb site to the P−O−CH_3 group; (c) like (a) but bonding at the type IIIa site; (d) like (b) but bonding to the type IIIa site. The numbered dashed lines show the H-bonding interactions, corresponding to Table 4. (1) and (1′) are OH···O bonds and (2) and (3) are CH···O bonds. In (d), bond (2) is partially obscured by the Al(T_d) atom.

data,[57a,59a] for DMMP adsorption on partially hydroxylated γ-Al_2O_3, strictly on the basis of the better agreement between the observed $\Delta\nu$(P=O) and that computed for dative bonding. Nevertheless the results are consistent with the conclusion, based on ΔE_{ads}, that dative bonding is favored over H-bonding when vacant Al(T_d) sites are available. Similar conclusions were reached by Templeton and Weinberg[59a] who found that Al···O=P bonding is energetically favored over OH···O=P bonding but gives about the same $\Delta\nu$(P=O). H-bonding, although relatively weak, can occur when OH groups are present and is the only mode of adsorption on a fully hydroxylated surface. The IR spectrum[62] of Sarin on γ-Al_2O_3 is essentially independent of whether or not OH groups are removed by evacuation at 900 °C prior to adsorption. This also suggests that adsorption can occur at both Al and OH sites and that the two cannot easily be distinguished solely in terms of the internal vibrational modes of the adsorbate.

Finally, a calculation was performed for adsorption at the type IIIb site of the $Al_{32}O_{48}$ 1,4 model in Figure 3b. H-bonds to the O atom of both the P=O and P−O−CH_3 groups were investigated. In either case geometry optimization resulted in movement of the molecule away from the OH site and toward one of the vacant Al(T_d) sites on the periphery of the cluster, where a dative bond then formed. This illustrates a point discussed above; namely, that such sites are preferred for adsorption when they are available (i.e., when not all Al(T_d) have formed type I sites). The results also indicate the reason why this initial series of calculations, aimed mainly at a comparison of adsorption at different types of OH sites, was performed using the small Al_8O_{12} cluster for which the only surface Al(T_d) site is occupied by an OH.

5.2.1.2. Sarin and VX. The adsorption of Sarin and VX on the Al_8O_{12} cluster was evaluated in the same manner as for DMMP. In view of the DMMP results, attention was focused on interactions between the type IIIb OH and either type of O atom (alkoxy or phosphonyl) and on the bonding of F (Sarin), N (VX), or S(VX) to either of the two OH sites. The results, shown in Table 3, are consistent with those for DMMP. Bonding via the interaction of the P=O group with the type IIIb OH is the most favorable mechanism. The AIM analyses (not shown) were consistent with those in Table 4. The trends in ρ and $\nabla^2\rho$ at the 3,-1 bond critical points reflected those in ΔE_{ads}, with the major contribution coming from the bond between the type IIIb OH and the O atom of the phosphonyl or the alkoxy group. In the case of Sarin adsorption via a weak OH···F bond, a large fraction of the small ΔE_{ads} derived from an additional CH···O bond. Bonding of VX via an OH···S bond at the type I site gave a very slightly endothermic ΔE_{ads} of +0.34 kcal/mol suggesting a very weakly bound metastable state. A more accurate description, in this case, may require geometry optimization using a GGA-XC functional[96] appropriate to noncovalent interactions.

It is noted that the trend in the type IIIb OH···O=P bond energy (DMMP > Sarin > VX) parallels that for the Al(T_d)···O=P bond on the OH-free surface (Table 2). However, the energy differences are in all cases small, and small secondary contributions from C−H···O interactions make a detailed comparison difficult. Calculations of the vibrational modes gave $\Delta\nu$(P=O) = −63 and −84 cm^{-1} respectively, relative to the computed gas-phase frequencies, for Sarin and VX adsorbed via a type IIIb OH···O=P bond. These are comparable to the corresponding value of −78 cm^{-1} obtained above for DMMP. The VX result is also close to the value of −95 cm^{-1} (Table 2) obtained for dative bonding to the OH-free surface.

An interesting effect was observed when attempting to adsorb VX via an OH···N bond at the type IIIb site. Geometry relaxation led to transfer of the proton to the N to give the corresponding ammonium ion. The reaction energy of −18.8 kcal/mol (uncorrected for BSSE) was somewhat less than the (uncorrected) value of ΔE_{ads} = −24.5 kcal/mol for the type IIIb OH···O=P bond. This is an unexpected result, given that experiment[97] shows that adsorption of pyridine on hydroxylated γ-Al_2O_3 does not yield a pyridinium ion. This led to an examination of the proton affinities (PAs) of pyridine, 2,6-dimethyl pyridine (2,6-DMP) and VX. 2,6-DMP is of interest since it gives evidence[97] of being a sufficiently strong base to form the corresponding pyridinium ion when adsorbed on

TABLE 4: AIM Analysis of Selected H-Bonded Structures for Adsorbed DMMP[a]

structure	ΔE_{ads}	bond	r(O···H) [b]	r(C···O) [b]	∠(O···H-X) [c]	ρ	$\nabla^2\rho$
Figure 6a	−23.2	1	1.451		166	0.081	0.129
		2	2.143	3.216	163	0.018	0.061
		3	2.295	3.349	160	0.013	0.046
Figure 6b	−13.9	1	1.580		170	0.062	0.128
		2	2.351	3.333	147	0.012	0.041
		3	2.261	3.254	149	0.015	0.051
Figure 6c	−13.7	1	1.493		174	0.072	0.130
		2	2.161	3.165	151	0.017	0.062
		3	2.394	3.419	155	0.011	0.039
Figure 6d	−9.9	1	1.670		174	0.048	0.119
		1'	2.105		148	0.018	0.066
		2	2.340	3.409	163	0.012	0.042
		3	2.269	3.337	164	0.015	0.048

[a] ΔE_{ads} in kcal/mol (cf. Table 3); ρ (charge density at the "3,-1" critical point) and $\nabla^2\rho$ (Laplacian of charge density at the critical point) in atomic units. The bond numbers refer to Figure 6. [b] Interatomic distances in Å. r(O···H) is the length of the H-bond. r(C···O) is the distance from C to O in the C−H···O bond. [c] O···H−O (bond 1,1′) or O···H−C (bond 2, 3) angle in degrees.

γ-Al_2O_3. The PA of an amine XN at finite temperature (T) is defined as the enthalpy change, $\Delta H(T)$, for the gas-phase reaction $XN + H^+ \rightarrow XN{-}H^+$ and is given by

$$\Delta E_{PA} = E(XN{-}H^+) - E(XN) - E(H^+)$$

$$\Delta H(T) = \Delta E_{PA} + E_{TRV}(XN{-}H^+) - E_{TRV}(XN) - (5/2)RT$$

Here $E(XN{-}H^+)$ and $E(XN)$ are the relaxed electronic energies of the protonated and the bare amine, and E_{TRV} is the total translational, rotational and vibrational energy. The (5/2)RT accounts for the H^+ translational energy and for the Δ(PV) contribution. In this definition, a negative $\Delta H(T)$ indicates an exothermic process.

The experimental[98] PAs of gas-phase pyridine and 2,6-DMP at room temperature are $\Delta H(298) = -930$ and -963 kJ/mol respectively. The values computed here for pyridine, 2,6-DMP and VX are −926.0, −963.2, and −986.4 kJ/mol respectively. The pyridine result is also in good agreement with the value of −935.5 kJ/mol obtained[99] at the B3LYP/6-311$^+$G(2df,p) level. The computed $\Delta H(298)$ for the amine group in VX is also close to the experimental values[98] for other trialkyl amines such as triethyl- and tripropylamine (−981.8 and −991.0 kJ/mol respectively). These results indicate that the VX amine group is more basic than 2,6-DMP and should thus be able to deprotonate acidic sites on the γ-Al_2O_3 surface.[97] It is noted that ΔE_{dp} for the OH site (Table 1) is larger in magnitude than ΔE_{PA}. However, ΔE_{dp} as defined above includes a large contribution (on the order of several hundred kJ/mol) from the energy required to separate the Al−O$^-$ and the H^+ to infinity. Hence ΔE_{dp} greatly overestimates the energetic cost to move the H^+ to the nearby (adsorbed) VX molecule.

5.2.2. $Al_{32}O_{48}$ Cluster. This section builds on the work described above by treating adsorption on a fully hydroxylated surface, one in which multiple OH···O═P and CH···O bonds are possible. Previous work[24] on the adsorption of phosphonyl species on the hydroxylated a-SiO_2 surface indicated that formation of *two* Si−OH···O═P bonds to a single P═O group is the energetically favored mode of adsorption. It is of interest to determine whether this model can be extended to γ-Al_2O_3.

These calculations employed the $Al_{32}O_{48}$ cluster with all seven "surface" Al(T_d) sites (cf. Figure 3b) converted to type I OH sites. This was done to inhibit the preferential formation of an Al(T_d)···O═P bond which occurs during adsorption of DMMP when empty Al(T_d) sites are available (see above). The seven accompanying H atoms were placed on surface O atoms to form type III sites. Six of these were placed on O_a sites to form 1,2 configurations with the peripheral type I sites. The seventh was placed on an O_b site to form a 1,4 configuration with the central type I Al-OH site. The atoms involved are labeled "(1)" and "O_b(4)" in Figure 3b. This adsorption site, which is used in subsequent calculations, thus resembles that studied for the Al_8O_{12} cluster but is now located at the center of a fully hydroxylated surface. Geometry optimization included the adsorbed molecule (if any), all the added H and OH, all seven surface Al atoms and all surface O atoms to which an H had been added.

A point of concern, for a complex system such as this, is whether a true global energy minimum is located in the relaxation process. As a test, two sets of DMMP calculations were done. One began with a cluster which had been previously relaxed when bare. The other began with the cluster in a configuration which was far from relaxed, with all atoms in bulk-lattice positions and all O−H and Al−O−H bonds normal to the surface. In either case, bonding of the phosphonyl O atom to the central type I OH and to the adjacent type IIIb site were treated. For adsorption at the type I site the relaxed energy minimum was independent of the starting configuration to within 0.05 kcal/mol. For the type III site, adsorption on the previously relaxed cluster gave an energy minimum that was slightly lower (i.e., more stable), by 0.84 out of 23.2 kcal/mol (see below).

For DMMP and Sarin the structures and adsorption energies were very similar to those obtained above for the Al_8O_{12} cluster. For DMMP adsorption *via* an OH···O═P bond, $\Delta E_{ads} = -23.2$ (−7.2) kcal/mol was found for the type IIIb (type I) site. These can be compared to the values of −23.2 and −4.5 kcal/mol, respectively, obtained for the hydroxylated Al_8O_{12} cluster (Table 3). For Sarin an OH···O═P bond at the type IIIb site gave $\Delta E_{ads} = -18.2$ kcal/mol vs −21.9 kcal/mol (Table 3) for the Al_8O_{12} cluster. As in the case of the Al_8O_{12} cluster, AIM analysis showed the formation of a few CH···O bonds with ∼70% of the total ΔE_{ads} coming from the type IIIb OH···O═P bond.

The results showed no indication of bonding of the $P = O$ to more than one OH group, in contrast to the case of hydroxylated a-SiO_2 noted above. The reason for this is not obvious. It is speculated that, because a type III OH is back-bonded to three Al atoms, it lacks the freedom of motion available to an OH on a-SiO_2, which is back-bonded to only one Si. This prevents the type III OH from relaxing into a configuration in which an optimum OH···O distance and bond angle can be achieved simultaneously for two H-bonds to a single P═O group.

For the fully hydroxylated $Al_{32}O_{48}$ cluster, severe steric hindrance was encountered when attempting to adsorb VX, in the vapor-phase configuration shown in Figure 1c, *via* a type IIIb OH···O═P bond. This results from one of the isopropyl groups preventing the phosphonyl O atom from approaching sufficiently close to the OH group (see Supporting Information). The resulting bonding interaction is negligibly small ($\Delta E_{ads} \approx -1$ kcal/mol before BSSE correction), presumably because the steric repulsion effectively neutralizes the contribution from the weak OH···O and CH···O bonds (identified in AIM analysis) that are able to form. The Supporting Information discusses rotational isomerization in the isolated VX molecule which, to our knowledge, has not been analyzed previously. Steric hindrance does not, however, affect formation of the Al(T_d)···O═P dative bond on the OH-free surface since in this case the bonding geometry (cf. Figure 5c) keeps the amine group well away from the surface, even for the larger $Al_{32}O_{48}$ cluster.

In order to facilitate adsorption on the fully hydroxylated $Al_{32}O_{48}$ cluster, the free VX molecule was placed into a more favorable configuration, as described in the Supporting Information. This was only ~2 kcal/mol higher in energy than that shown in Figure 1c; however, the configuration (chosen to minimize steric hindrance) corresponds to a relatively deep local minimum in energy. A BSSE-corrected ΔE_{ads} of −11.5 kcal/mol was found for adsorption *via* a type IIIb OH···O═P bond. Unlike the case for DMMP and Sarin discussed above, this is significantly smaller in magnitude than the result (−19.0 kcal/mol, Table 3) for the same adsorption site on the hydroxylated Al_8O_{12} cluster. Only a small part of this difference can be explained by the ~2 kcal/mol difference in free-molecule energies. It is speculated that the remaining discrepancy results from steric effects, which prevent complete relaxation of the adsorbed molecule, or from the fact that the adsorbed VX may be "trapped" in a local energy minimum lying significantly higher than the true minimum. Locating the global-minimum-energy for a large molecule like VX on hydroxylated γ-Al_2O_3 will require a molecular dynamics treatment at finite temperature.

5.3. Electronic Excitation. Tables S1−S3 in the Supporting Information show TDDFT results (transition energies and oscillator strengths) for dipole-allowed (singlet → singlet) transitions of the gas-phase species. The main concern is with transitions lying closest to the near-UV edge of the TSS (Figure 7); hence, Tables S1−S3 show only the twelve lowest-energy excitations. As noted above, there are few experimental data for the electronic excitation of these species. In the absence of such data, results obtained using *ADF* and *Gaussian* as described above were compared. In the latter case the molecular geometry was first optimized at the B3LYP/6-311^{++}G(d,p) level. In general the agreement between the two sets of TDDFT results, obtained using different functionals and basis sets, is quite good. Those obtained using SAOP are considered more reliable since this functional was specifically designed[44] to model electronic excitation. The results all pertain to $T = 0$ K with the molecule frozen in the lowest-energy ground-state configuration. Including the effects of finite temperature[100] can lead to shifts in the transition energies which are not taken into account here. However, these effects are not large enough to preclude the central goal of determining the overlap of the computed spectra with the TSS.

For free DMMP the onset of absorption is computed to lie at 7.12 eV. The low-energy transitions correspond to n → σ* excitations of nonbonding orbitals (NBOs) on the phosphonyl and methoxy O atoms and lie well outside the region of significant TSS intensity. The results are consistent with the available data[70] which show no absorption (except for possible impurities) below 6.2 eV. The Sarin results are similar except that the absorption onset lies somewhat higher, at 7.38 eV. For free VX, on the other hand, the computed absorption onset is at 4.16 eV. All transitions in Table S3 involve excitation of NBOs on the N and/or S atoms, and the threshold transition is an n → σ* excitation of the N atom. For VX in ethanol[74] the lowest-energy peak is at 4.66 eV. A blue shift relative to the gas-phase is expected[101] in a solvent such as ethanol which can lower the energy of the ground-state by forming an H-bond with the NBO on the N atom.

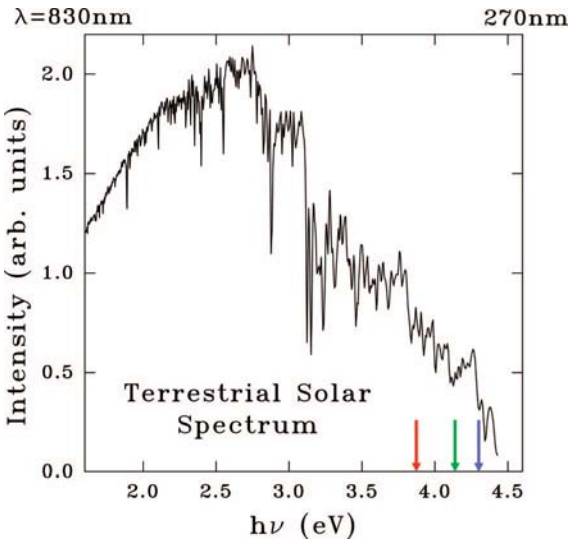

Figure 7. The terrestrial solar spectrum from the near-infrared to the near-ultraviolet (ref 69) with arrows marking the computed onset of electronic excitation (at 0 °K) for free VX (green), for VX adsorbed on OH-free γ-Al_2O_3 (red), and for VX adsorbed on hydroxylated γ-Al_2O_3 (blue). The scale is linear in energy, and the corresponding wavelengths at the end points are given.

For molecules adsorbed on the OH-free Al_8O_{12} cluster, the excitation threshold was determined by identifying the lowest-energy transition for which the initial and final states are MOs composed largely of atomic orbitals (AOs) associated with the molecule (see below). For DMMP, the threshold shifts to 7.88 eV from 7.12 eV for the free molecule (Table S1). For Sarin, it shifts to 8.13 eV from 7.38 eV for the free molecule (Table S2). The origin of these shifts (~0.75 eV in either case) has been examined in terms of the MOs involved. For the free molecule, the HOMO and HOMO-1 are nearly degenerate and are formed largely from NBOs on the phosphonyl O atom. In the adsorbed state, dative-bond formation shifts these to lower energy by 1.1 eV or more, and an MO composed of NBOs on the alkoxy O atom(s) then becomes the HOMO. This MO, which is not directly involved in adsorption, lies a few tenths of an eV lower in energy than the free-molecule HOMO. The LUMO of the adsorbed molecule, on the other hand, lies slightly higher in energy than that of the free molecule. The net effect of these adsorption-induced shifts is the blue shift in the excitation threshold.

The computed HOMO−LUMO gap of the bare Al_8O_{12} cluster (with PHT) is 4.4 eV (ref 25) vs the experimental[68] γ-Al_2O_3 band gap of 7.2 eV. Hence, the TDDFT calculations yield many low-energy transitions between cluster levels as well as charge-transfer transitions in which the initial state is an MO localized mainly on the molecule and the final state an MO localized mainly on the cluster (or vice versa). These have been ignored in analyzing the TDDFT results. The MOs involved in the near-

threshold internal excitations of adsorbed DMMP and Sarin are composed almost purely of AOs associated with the molecule (as opposed to the cluster) with, in the case of the molecular LUMO, a small contribution from p orbitals on the Al(T_d) adsorption site. Thus the calculated threshold for internal excitation of the adsorbate should not be strongly affected by the DFT underestimation of the γ-Al_2O_3 band gap. It is noted in passing that the excitation thresholds for DMMP and Sarin are fairly close to the actual γ-Al_2O_3 band gap (7.2 eV). Depending on the alignment of the molecular HOMO and LUMO with the γ-Al_2O_3 band edges, charge-transfer effects may occur experimentally in photoexcitation of the adsorbed species.

For VX (also adsorbed via a P═O···Al bond) the threshold red-shifts to 3.87 eV from the free-VX value of 4.16 eV. The threshold transition is the n → σ* excitation of the NBO on the N atom, as for the free molecule. This orbital, which is not directly involved in chemisorption, is essentially unaffected by adsorption. The LUMO of adsorbed VX lies slightly lower than that of the free molecule which then gives rise to the computed red-shift. For VX adsorbed via an OH···O═P bond at a type IIIb OH site the threshold is found at 4.31 eV. For completeness, excitation of a free VX molecule protonated on the N atom was also considered. As noted above, the amine group in VX is able to undergo a Brønsted acid−base reaction with an acidic OH site. As expected, this eliminates the n → σ* excitation of the N atom, and the n → σ* excitation of the S atom, at 5.17 eV, then becomes the threshold transition. The VX results are included in Figure 7 which shows that solar photoexcitation is a significant possibility. It is known[102] that n → σ* excitation of the N atom in tertiary amines leads to homolytic dissociation of alkyl C−N bonds into free-radical fragments which can then undergo further reaction, and experiment[74] shows that irradiation of VX in the vapor phase at 4.89 eV leads to molecular rearrangement. The TDDFT results also indicate that protonated VX should be significantly less photosensitive to the TSS.

6. Summary

The adsorption and photoexcitation of DMMP, Sarin, and VX on OH-free and hydroxylated γ-Al_2O_3 surfaces have been studied computationally using DFT and Al_8O_{12} and $Al_{32}O_{48}$ clusters terminated with pseudo-H. The design and testing of these clusters are important components of the overall study. The results are as follows.

(1) New results for the adsorption of VX on OH-free γ-Al_2O_3 are consistent with previous results for DMMP and Sarin. Adsorption via an Al···O═P dative bond at an unsaturated Al(T_d) site is favored over Al···N or Al···S dative bonding. These are believed to be the first computational results for VX adsorption on any surface.

(2) Various issues have been examined which are important in constructing cluster models for the hydroxylated γ-Al_2O_3 surface. These include the configuration of different types of OH sites and the identification of the sites involved in chemisorption. The models have been evaluated by comparing ΔE_{ads} for dissociative adsorption of H_2O with 2-DPS results, and good agreement is obtained even for the small cluster. However, ΔE_{ads} shows a dependence on the coordination of the type III OH site which is not seen in the 2-DPS results.

(3) The valence-band DOS for the hydroxylated γ-Al_2O_3 surface, computed using a 2-DPS model, has been compared with photoemission data. Type III OH sites give a state lying just below the bottom of the O 2p band which can be seen in SXPS. The SXPS feature was not previously assigned to a particular OH site. Type I sites give Al−OH (AlO−H) states near the top (bottom) of the O 2p band which are obscured in SXPS by the bulk Al_2O_3 emission. The DOS results for both the large and small clusters are in good agreement with those of 2-DPS calculations.

(4) Deprotonation energies computed for the type I and type III OH sites confirm that the latter is more acidic. Removing a proton from the type I site, followed by geometry relaxation, leads to reprotonation *via* transfer of H^+ from the type III OH site. Similar deprotonation energies are obtained for both the large and small clusters.

(5) Bonding between a type III OH and the O atom of the P═O group is the favored mode of adsorption for all three reagents on the hydroxylated surface. Bonding to a type I OH is weak, in agreement with IR spectroscopy experiments showing that type I sites are not active in the initial adsorption of DMMP or Sarin. The computed room-temperature enthalpy of adsorption of DMMP via a type IIIb OH···O═P bond agrees well with an experimental estimate for DMMP bonding to a $-CO_2H$-terminated alkanethiolate SAM. However, even the strongest OH···O═P bond is much weaker than an Al(T_d)···O═P dative bond on the OH-free surface. The latter mode of bonding will occur whenever vacant Al(T_d) sites are available.

(6) Unlike in the case of hydroxylated a-SiO_2 there is no tendency of the phosphonyl O atom to bond to more than one OH group. It is speculated that the type III OH site lacks sufficient freedom of motion to permit the H-bond distance and angle requirements to be satisfied simultaneously for two OH···O═P bonds to a single O═P group.

(7) H-bonding to the P═O group causes a red-shift in the ν(P═O) stretching mode. $\Delta\nu$(P═O) is comparable to that seen, either experimentally or computationally, for Al(T_d)···O═P bonding even though the H-bond is considerably weaker than the dative bond. This indicates, in agreement with experiment, that the two modes of adsorption cannot be distinguished solely by means of the vibrational spectrum of the adsorbate.

(8) The amine group in VX is able to extract a proton from an acidic type III OH site to form the corresponding ammonium ion. The estimated reaction energy of −18.8 kcal/mol is only somewhat less than the energy of the strongest H-bond found in this study. Computed proton affinities show that the VX amine group is a stronger base than either pyridine or 2,6-dimethyl pyridine and is comparable in basicity to triethyl- and tripropylamine.

(9) C−H···O bonds between CH_3 groups and O atoms, either in the Al_2O_3 surface or at an OH site, are formed in all cases studied. However, AIM analyses show that these are weak in comparison to type III OH···O═P bonds.

(10) The energy surface of VX is complex, and identification of the global-minimum-energy configuration is difficult for either the free or adsorbed species. Adsorption on the larger ($Al_{32}O_{48}$) hydroxylated cluster, and presumably on a hydroxylated semi-infinite surface, is strongly affected by steric hindrance. For geometric reasons, such factors are less important for Al(T_d)···O═P bonding on the OH-free surface. For DMMP and Sarin (for which steric effects appear to be less important), adsorption on the hydroxylated Al_8O_{12} and $Al_{32}O_{48}$ clusters give similar results.

(11)For DMMP and Sarin, either in the gas phase or adsorbed on OH-free γ-Al_2O_3, the threshold electronic excitation falls in the vacuum-UV (∼7.1 eV or higher), well above the cutoff of the terrestrial solar spectrum (∼4.5 eV). However, VX excitation begins near 4.2 eV in the gas phase and near 3.9 eV when

adsorbed via an Al(T_d)···O═P dative bond on the OH-free surface. Adsorption via an OH···O═P bond shifts the VX absorption onset to about 4.3 eV, slightly higher than the gas-phase value. Adsorption-induced changes in the excitation thresholds for all three species have been analyzed in terms of shifts in MOs. The different excitation thresholds for VX all lie within range of the terrestrial solar spectrum which suggests that photochemistry induced by sunlight is a real possibility.

Acknowledgment. This work was supported by the Defense Threat Reduction Agency (DTRA). Computer facilities were provided by the Naval Research Laboratory and by the DOD High-Performance Computing Modernization Program at the AFRL-MSRC, Wright-Patterson AFB. S.C. Badescu is thanked for help with the *XAIM* installation. J. C. Baum is thanked for helpful discussion on solvent effects in molecular electronic spectra. E. V. Patterson is thanked for providing the optimized structure for free VX in advance of publication and for helpful discussions on VX isomerization, and D. C. Sorescu is thanked for helpful communications regarding geometry optimization. Communications with H. P. Pinto concerning the structure of γ-Al_2O_3 are gratefully acknowledged.

Supporting Information Available: Electron-counting and pseudohydrogens, rotational isomerization in VX, and optical excitations in free DMMP, Sarin, and VX. This material is available free of charge via the Internet at http://pubs.acs.org.

References and Notes

(1) Daniel, K. A.; Kopff, L. A.; Patterson, E. V. *J. Phys. Org. Chem.* **2008**, *21*, 321.
(2) Soares, T. A.; Osman, M. A.; Straatsma, T. P. *J. Chem. Theory Comput.* **2007**, *3*, 1569.
(3) Menke, J. L.; Patterson, E. V. *J. Mol. Struct. (Theochem)* **2007**, *811*, 281.
(4) Majumdar, D.; Roszak, S.; Leszczynski, J. *Mol. Phys.* **2007**, *105*, 2551.
(5) Wang, J.; Gu, J.; Leszczynski, J.; Feliks, M.; Sokalski, W. A. *J. Phys. Chem. B* **2007**, *111*, 2404.
(6) Wang, J.; Gu, J.; Leszczynski, J. *J. Phys. Chem. B* **2006**, *110*, 7567.
(7) Bandyopadhyay, I.; Kim, M. J.; Lee, Y. S.; Churchill, D. G. *J. Phys. Chem. A* **2006**, *110*, 3655.
(8) Paukku, Y.; Michalkova, A.; Majumdar, D.; Leszczynksi, J. *Chem. Phys. Lett.* **2006**, *422*, 317.
(9) Šečkutė, J.; Menke, J. L.; Emnett, R. J.; Patterson, E. V.; Cramer, C. J. *J. Org. Chem.* **2005**, *70*, 8649.
(10) Kaczmarek, A.; Gorb, L.; Sadlej, A. J.; Leszczynski, J. *J. Struct. Chem.* **2004**, *15*, 517.
(11) Zheng, F.; Zhan, C.-G.; Ornstein, R. L. *J. Chem. Soc., Perkin Trans. 2* **2001**, 2355.
(12) Walker, A. R. H.; Suenram, R. D.; Samuels, A.; Jensen, J.; Ellzy, M. W.; Lochner, J. M.; Zeroka, D. *J. Mol. Spectrosc.* **2001**, *207*, 77.
(13) Patterson, E. V.; Cramer, C. J. *J. Phys. Org. Chem.* **1998**, *11*, 232.
(14) Albaret, C.; Lacoutière, S.; Ashman, W. P.; Froment, D.; Fortier, P.-L. *Proteins: Struct., Funct., Genetics* **1997**, *28*, 543.
(15) Rauk, A.; Shishkov, I. F.; Vilkov, L. V.; Koehler, K. F.; Kostyanovsky, R. G. *J. Am. Chem. Soc.* **1995**, *117*, 7180.
(16) Politzer, P.; Jayasuriya, K.; Lane, P. *J. Mol. Struct. Theochem.* **1987**, *149*, 259.
(17) Politzer, P.; Jayasuriya, K. *J. Mol. Struct. Theochem.* **1986**, *134*, 381.
(18) Ewig, C. S.; Van Wazer, J. R. *J. Mol. Struct. Theochem.* **1985**, *122*, 179.
(19) Michalkova, A.; Gorb, L.; Ilchenko, M.; Zhikol, O. A.; Shishkin, O. V.; Leszczynski, J. *J. Phys. Chem. B* **2004**, *108*, 1918.
(20) Michalkova, A.; Ilchenko, M.; Gorb, L.; Leszczynski, J. *J. Phys. Chem. B* **2004**, *108*, 5294.
(21) Michalkova, A.; Martinez, J.; Zhikol, O. A.; Gorb, L.; Shishkin, O. V.; Leszczynska, D.; Leszczynski, J. *J. Phys. Chem. B* **2006**, *110*, 21175.
(22) Michalkova, A.; Paukku, Y.; Majumdar, D.; Leszczynski, J. *Chem. Phys. Lett.* **2007**, *438*, 72.
(23) Bermudez, V. M. *J. Phys. Chem. C* **2007**, *111*, 3719.
(24) Bermudez, V. M. *J. Phys. Chem. C* **2007**, *111*, 9314.
(25) Bermudez, V. M. *Surf. Sci.* **2008**, *602*, 1938.
(26) Paukku, Y.; Michalkova, A.; Leszczynski, J. *Struct. Chem.* **2008**, *19*, 307.
(27) Suenram, R. D.; Lovas, F. J.; Plusquellic, D. F.; Lesarri, A.; Kawashima, Y.; Jensen, J. O.; Samuels, A. C. *J. Mol. Spectrosc.* **2002**, *211*, 110.
(28) Vishnyakov, A.; Neimark, A. V. *J. Phys. Chem. A* **2004**, *108*, 1435.
(29) Florián, J.; Štrajbl, M.; Warshel, A. *J. Am. Chem. Soc.* **1998**, *120*, 7959.
(30) Zhanpeisov, N. U.; Zhidomirov, G. M.; Yudanov, I. V.; Klabunde, K. J. *J. Phys. Chem.* **1994**, *98*, 10032.
(31) Ault, B. S.; Balboa, A.; Tevault, D.; Hurley, M. *J. Phys. Chem. A* **2004**, *108*, 10094.
(32) Munro, N. B.; Talmage, S. S.; Griffin, G. D.; Waters, L. C.; Watson, A. P.; King, J. F.; Hauschild, V. *Environ. Health Persp.* **1999**, *107*, 933.
(33) te Velde, G.; Bickelhaupt, F. M.; Baerends, E. J.; Fonseca Guerra, C.; van Gisbergen, S. J. A.; Snijders, J. G.; Ziegler, T. *J. Comput. Chem.* **2001**, *22*, 931.
(34) (a) Casarin, M.; Falcomer, D.; Vittadini, A. *Surf. Sci.* **2004**, *566*−*568*, 890. (b) Casarin, M.; Falcomer, D.; Glisenti, A.; Vittadini, A. *Inorg. Chem.* **2003**, *42*, 436. (c) Casarin, M.; Maccato, C.; Vittadini, A. *J. Phys. Chem. B* **2002**, *106*, 795.
(35) Casarin, M.; Maccato, C.; Vittadini, A. *Inorg. Chem.* **2000**, *39*, 5232.
(36) Taniike, T.; Tada, M.; Morikawa, Y.; Sasaki, T.; Iwasawa, Y. *J. Phys. Chem. B* **2006**, *110*, 4929.
(37) Sun, M.; Nelson, A. E.; Adjaye, J. *J. Phys. Chem. B* **2006**, *110*, 2310.
(38) Paglia, G.; Rohl, A. L.; Buckley, C. E.; Gale, J. D. *Phys. Rev. B* **2005**, *71*, 224115.
(39) Popelier, P. *Atoms in Molecules: An Introduction*; Pearson Education: Harlow, U.K., 2000.
(40) Bader, R. F. W. *Atoms in Molecules: A Quantum Theory*; Clarendon: Oxford, 1990.
(41) XAIM was developed by José Carlos Ortiz and Carles Bo; Univ. Rovira i Virgili; Tarragona, Spain (http://www.quimica.urv.es/XAIM/).
(42) Irikura, K. K.; Johnson, R. D., III; Kacker, R. N. *J. Phys. Chem. A* **2005**, *109*, 8430.
(43) Foresman, J. B.; Head-Gordon, M.; Pople, J. A.; Frisch, M. J. *J. Phys. Chem.* **1992**, *96*, 135.
(44) Schipper, P. R. T.; Gritsenko, O. V.; van Gisbergen, S. J. A.; Baerends, E. J. *J. Chem. Phys.* **2000**, *112*, 1344.
(45) Gaussian 03, Frisch, M. J.; Trucks, G. W.; Schlegel, H. B.; Scuseria, G. E.; Robb, M. A.; Cheeseman, J. R.; Montgomery, Jr., J. A.; Vreven, T.; Kudin, K. N.; Burant, J. C.; Millam, J. M.; Iyengar, S. S.; Tomasi, J.; Barone, V.; Mennucci, B.; Cossi, M.; Scalmani, G.; Rega, N.; Petersson, G. A.; Nakatsuji, H.; Hada, M.; Ehara, M.; Toyota, K.; Fukuda, R.; Hasegawa, J.; Ishida, M.; Nakajima, T.; Honda, Y.; Kitao, O.; Nakai, H.; Klene, M.; Li, X.; Knox, J. E.; Hratchian, H. P.; Cross, J. B.; Bakken, V.; Adamo, C.; Jaramillo, J.; Gomperts, R.; Stratmann, R. E.; Yazyev, O.; Austin, A. J.; Cammi, R.; Pomelli, C.; Ochterski, J. W.; Ayala, P. Y.; Morokuma, K.; Voth, G. A.; Salvador, P.; Dannenberg, J. J.; Zakrzewski, V. G.; Dapprich, S.; Daniels, A. D.; Strain, M. C.; Farkas, O.; Malick, D. K.; Rabuck, A. D.; Raghavachari, K.; Foresman. J. B.; Ortiz, J. V.; Cui, Q.; Baboul, A. G.; Clifford, S.; Cioslowski, J.; Stefanov, B. B.; Liu, G.; Liashenko, A.; Piskorz, P.; Komaromi, I.; Martin, R. L.; Fox, D. J.; Keith, T.; Al-Laham, M. A.; Peng, C. Y.; Nanayakkara, A.; Challacombe, M.; Gill, P. M. W.; Johnson, B.; Chen, W.; Wong, M. W.; Gonzalez, C.; Pople, J. A. *Gaussian 03*; Gaussian, Inc.: Wallingford CT, 2004.
(46) Mamaev, V. M.; Zernova, E. V.; Prisyazhnyuk, A. V.; Myshakin, E. M.; Berdyshev, D. V. *Dokl. Akad. Nauk* **1996**, *349*, 64 English transl.: *Dokl. Phys. Chem.* **1996**, *349*, 153.
(47) Strukov, O. G.; Utkina, S. V.; Petrunin, V. A.; Vlasova, Z. V.; Zavalishina, I. V.; Fadeev, V. N.; Kuntsevich, A. D.; Drozd, G. I. *Dokl. Akad. Nauk* **2001**, *380*, 784 English transl.: *Dokl. Phys. Chem.* **2001**, *380*, 247.
(48) Guilbault, G. G.; Scheide, E.; Das, J. *Spectrosc. Lett.* **1968**, *1*, 167.
(49) Bertilsson, L.; Potje-Kamloth, K.; Liess, H.-D.; Engquist, I.; Liedberg, B. *J. Phys. Chem. B* **1998**, *102*, 1260.
(50) Rusu, C. N.; Yates, J. T., Jr *J. Phys. Chem. B* **2000**, *104*, 12292.
(51) McGarvey, D. J.; Stuff, J. R.; Williams, B. R.; Durst, H. D. *Spectrosc. Lett.* **2000**, *33*, 795; **2001**, *34*, 253.
(52) Strukov, O. G.; Petrunin, V. A.; Kuntsevich, A. D.; Drozd, G. I. *Dokl. Akad. Nauk* **1997**, *357*, 216; English transl.: *Dokl. Chem.* **1997**, *357*, 267.
(53) Strukov, O. G.; Petrunin, V. A.; Fadeev, V. N.; Zavalishina, I. V.; Kuntsevich, A. D.; Drozd, G. I. *Dokl. Akad. Nauk* **2000**, *372*, 199; English transl.: *Dokl. Phys. Chem.*, **2000**, *372*, 72.
(54) Söderström, M. T.; Ketola, R. A. *Fresenius J. Anal. Chem.* **1994**, *350*, 162.

(55) Creasy, W. R.; Stuff, J. R.; Williams, B.; Morrissey, K.; Mays, J.; Duevel, R.; Durst, H. D. *J. Chromatogr. A* **1997**, *774*, 253.

(56) Farquharson, S.; Gift, A.; Maksymiuk, P.; Inscore, F. *Appl. Spectrosc.* **2005**, *59*, 654.

(57) (a) Mitchell, M. B.; Sheinker, V. N.; Mintz, E. A. *J. Phys. Chem. B* **1997**, *101*, 11192. (b) Sheinker, V. N.; Mitchell, M. B. *Chem. Mater.* **2002**, *14*, 1257.

(58) Aurian-Blajeni, B.; Boucher, M. M. *Langmuir* **1989**, *5*, 170.

(59) (a) Templeton, M. K.; Weinberg, W. H. *J. Am. Chem. Soc.* **1985**, *107*, 97. (b) *J. Am. Chem. Soc.* **1985**, *107*, 774.

(60) Davies, P. R.; Newton, N. G. *Appl. Surf. Sci.* **2001**, *181*, 296.

(61) Kim, C. S.; Lad, R. J.; Tripp, C. P. *Sens. Actuators B* **2001**, *76*, 442.

(62) Kuiper, A. E. T.; van Bokhoven, J. J. G. M.; Medema, J. *J. Catal.* **1976**, *43*, 154.

(63) van Bokhoven, J. J. G. M.; Kuiper, A. E. T.; Medema, J. *J. Catal.* **1976**, *43*, 168; *J. Catal.* **1976**, *43*, 181.

(64) Wagner, G. W.; Procell, L. R.; O'Connor, R. J.; Munavalli, S.; Carnes, C. L.; Kapoor, P. N.; Klabunde, K. J. *J. Am. Chem. Soc.* **2001**, *123*, 1636.

(65) Wagner, G. W.; Procell, L. R.; Munavalli, S. *J. Phys. Chem. C* **2007**, *111*, 17564 Wagner, G. W.; Itin, B. *J. Phys. Chem. C* **2008**, *112*, 9962.

(66) Trubitsyn, D. A.; Vorontsov, A. V. *J. Phys. Chem. B* **2005**, *109*, 21884.

(67) Moss, J. A.; Szczepankiewicz, S. H.; Park, E.; Hoffmann, M. R. *J. Phys. Chem. B* **2005**, *109*, 19779.

(68) French, R. H. *J. Am. Ceram. Soc.* **1990**, *73*, 477.

(69) Renewable Resource Data Center http://rredc.nrel.gov/solar/.

(70) Rewick, R. T.; Schumacher, M. L.; Haynes, D. L. *Appl. Spectrosc.* **1986**, *40*, 152.

(71) Sharpless, R. L.; Slanger, T. G. *Appl. Spectrosc.* **1989**, *43*, 570.

(72) Zuo, G.-M.; Cheng, Z.-X.; Shi, W.-P.; Zhang, X.-H.; Zhang, M. *J. Photochem. Photobiol. A: Chem.* **2007**, *188*, 143.

(73) Aschmann, S. M.; Tuazon, E. C.; Atkinson, R. *J. Phys. Chem. A* **2005**, *109*, 11828.

(74) Zuo, G.-M.; Cheng, Z.-X.; Li, G.-W.; Wang, L.-Y.; Chen, H. *J. Phys. Chem. A* **2005**, *109*, 6912.

(75) Ching, W. Y.; Ouyang, L.; Rulis, P.; Yao, H. *Phys. Rev. B* **2008**, *78*, 014106.

(76) Pinto, H. P.; Nieminen, R. M.; Elliott, S. D. *Phys. Rev. B* **2004**, *70*, 125402.

(77) (a) Pinto, H. P.; Elliott, S. D. *Mater. Res. Soc. Symp. Proc.* **2003**, *786*, E5. 21. (b) Pinto, H. P., personal communication.

(78) Figure 2 was constructed using the VENUS set of programs provided by R.A. Dilanian and F. Izumi at http://homepage.mac.com/fujioizumi/visualization/VENUS.html.

(79) Knözinger, H.; Ratnasamy, P. *Catal. Rev. - Sci. Eng.* **1978**, *17*, 31.

(80) Busca, G.; Lorenzelli, V.; Ramis, G.; Willey, R. J. *Langmuir* **1993**, *9*, 1492.

(81) Morterra, C.; Magnacca, G. *Catal. Today* **1996**, *27*, 497.

(82) Tsyganenko, A. A.; Mardilovich, P. P. *J. Chem. Soc. Faraday Trans.* **1996**, *92*, 4843.

(83) (a) Liu, X.; Truitt, R. E. *J. Am. Chem. Soc.* **1997**, *119*, 9856. (b) Liu, X. *J. Phys. Chem. C* **2008**, *112*, 5066.

(84) (a) Digne, M.; Sautet, P.; Raybaud, P.; Euzen, P.; Toulhoat, H. *J. Catal.* **2002**, *211*, 1. (b) *J. Catal.* **2004**, *226*, 54.

(85) Dyan, A.; Cenedese, P.; Dubot, P. *J. Phys. Chem. B* **2006**, *110*, 10041.

(86) Handzlik, J. *Surf. Sci.* **2007**, *601*, 2054.

(87) Rhodin, T. N.; Merrill, R. P.; O'Hagan, P. J.; Woronick, S. C.; Shinn, N. D.; Woolery, G. L.; Chester, A. W. *J. Phys. Chem.* **1994**, *98*, 2433.

(88) Nortier, P.; Borosy, A. P.; Allavena, M. *J. Phys. Chem. B* **1997**, *101*, 1347.

(89) Kawakami, H.; Yoshida, S. *J. Chem. Soc. Faraday Trans. 2* **1986**, *82*, 1385.

(90) Koch, U.; Popelier, P. L. A. *J. Phys. Chem.* **1995**, *99*, 9747.

(91) Sosa, G. L.; Peruchena, N.; Contreras, R. H.; Castro, E. A. *J. Mol. Struct.: THEOCHEM* **1997**, *401*, 77.

(92) Jensen, S. J. K.; Tang, T.-H.; Csizmadia, I. G. *J. Phys. Chem. A* **2003**, *107*, 8975.

(93) Desiraju, G. R. *Acc. Chem. Res.* **1991**, *24*, 290; **1996**, *29*, 441.

(94) Taylor, R.; Kennard, O. *J. Am. Chem. Soc.* **1982**, *104*, 5063.

(95) Rozas, I. *Phys. Chem. Chem. Phys.* **2007**, *9*, 2782.

(96) Zhao, Y.; Truhlar, D. G. *Acc. Chem. Res.* **2008**, *41*, 157; *Theor. Chem. Acc.* **2008**, *129*, 215.

(97) Vimont, A.; Lavalley, J. C.; Sahibed-Dine, A.; Otero Areán, C.; Rodríguez-Delgado, M.; Daturi, M. *J. Phys. Chem. B* **2005**, *109*, 9656.

(98) Hunter, E. P. L.; Lias, S. G. *J. Phys. Chem. Ref. Data* **1998**, *27*, 413.

(99) Despotović, I.; Kovačević, B.; Maksić, Z. B. *New J. Chem.* **2007**, *31*, 447.

(100) Besley, N. A.; Oakley, M. T.; Cowan, A. J.; Hirst, J. D. *J. Am. Chem. Soc.* **2004**, *126*, 13502.

(101) Stevenson, D. P. *J. Am. Chem. Soc.* **1962**, *84*, 2849.

(102) Calvert, J. G.; Pitts, J. N., Jr. *Photochemistry*; Wiley: New York, 1966.

JP809053U